Field-Induced Tuning of the Pairing State in a Superconductor

A. Rosuel, C. Marcenat, G. Knebel, T. Klein, A. Pourret, N. Marquardt, Q. Niu, S. Rousseau, A. Demuer, G. Seyfarth, et al.

Field-Induced Tuning of the Pairing State in a Superconductor

A. Rosuel,[1] C. Marcenat,[1] G. Knebel,[1] T. Klein,[2] A. Pourret,[1] N. Marquardt,[1] Q. Niu,[1,3] S. Rousseau,[1] A. Demuer,[4] G. Seyfarth,[4] G. Lapertot,[1] D. Aoki,[5] D. Braithwaite,[1] J. Flouquet,[1] and J. P. Brison[1,*]

[1]*Univ. Grenoble Alpes, CEA, Grenoble-INP, IRIG, Pheliqs, 38000 Grenoble, France*
[2]*Univ. Grenoble Alpes, CNRS, Institut Néel, 38000 Grenoble, France*
[3]*Anhui Key Laboratory of Condensed Matter Physics at Extreme Conditions, High Magnetic Field Laboratory, HFIPS, Anhui, Chinese Academy of Sciences, Hefei 230031, China*
[4]*Univ. Grenoble Alpes, INSA Toulouse, Univ. Toulouse Paul Sabatier, EMFL, CNRS, LNCMI, Grenoble 38042, France*
[5]*IMR, Tohoku University, Oarai, Ibaraki 311-1313, Japan*

(Received 10 May 2022; revised 14 October 2022; accepted 13 January 2023; published 22 February 2023)

The recently discovered superconductor UTe_2, with a superconducting transition temperature T_c between 1.5 and 2 K, is attracting much attention due to strong suspicion of spin-triplet and topological superconductivity. Its properties under magnetic field are also remarkable, with field-reinforced ($H\|b$) and field-induced [H in the (b,c) plane] superconducting phases. Here, we report the first complete thermodynamic determination of the phase diagram for fields applied along the three crystallographic directions. For field along the easy a axis, we uncover a strong negative curvature of the upper critical field very close to T_c, revealing a strong suppression of the pairing strength at low magnetic fields. By contrast, measurements performed up to 36 T along the hard magnetization b axis confirm a bulk field-reinforced superconducting phase. Most of all, they also reveal the existence of a phase transition line within the superconducting phase. Drastic differences occur between the low-field and high-field phases pointing to different pairing mechanisms. Detailed analysis suggests a possible transition between a low-field spin-triplet to high-field spin-singlet state, a unique case among superconductors.

DOI: 10.1103/PhysRevX.13.011022

Subject Areas: Condensed Matter Physics, Strongly Correlated Materials, Superconductivity

I. INTRODUCTION

The major breakthrough of the past 40 years in the field of superconductivity has been the discovery of several families of unconventional superconductors: heavy fermions, organics, high-T_c cuprates, and iron pnictides in chronological order. All are controlled by pairing mechanisms dominated by purely electronic interactions instead of the conventional electron-phonon interaction. These new pairing mechanisms also lead to new superconducting states, with different possible spin states (spin-singlet–even parity or spin-triplet–odd parity), and corresponding orbital states, dubbed d wave, p wave, and f wave. Spin-triplet superconductivity is presently highly sought after in the context of quantum engineering, as the required starting point to build robust topologically protected qubits. Artificial heterostructures have been proposed to create this rare state from conventional s-wave superconductors [1]. However, experimental success following this line remains controversial. Hence, bulk spin-triplet superconductors with strong spin-orbit coupling is an appealing alternative.

Besides superfluid ^{3}He [2], a perfect analog of a neutral spin-triplet p-wave superconductor below 3 mK, most candidates for bulk spin-triplet superconductivity are found among uranium-based heavy-fermion systems. The most famous is undoubtedly UPt_3, which is one of the rare systems showing not only one superconducting phase, but three superconducting phases differing by their symmetries [3]. Another major series of systems is that of UGe_2, URhGe, and UCoGe, where the bulk coexistence of ferromagnetism and superconductivity leaves little doubt that they are also spin-triplet superconductors. They all display in addition uncommon superconducting phase diagrams, with a reentrance or reinforcement of superconductivity under large magnetic fields [4].

*Corresponding author.
jean-pascal.brison@cea.fr

Naturally, these uranium heavy-fermion superconductors are also central in modern condensed matter physics, as potential topological superconductors. For example, UPt_3 is also considered as a prime candidate for topological chiral spin-triplet superconductivity, like URu_2Si_2 is a prime candidate for topological chiral spin-singlet (d-wave) superconductivity [5].

However, spin-triplet superconductivity remains a rare state of matter, with no clear understanding of the main reasons driving its appearance. In this context, the discovery of superconductivity in UTe_2 above 1.5 K back in 2018 [6] drove much enthusiasm in the condensed matter physics community. UTe_2 is a stunning system for almost all of its properties, starting with the fact that it is metallic only thanks to strong electronic correlations [7–9]. Its superconductivity shows extraordinary robustness to very large magnetic fields [6,10–12], a feature also associated to the ferromagnetic superconductors, and requiring at least spin-triplet superconductivity. Still UTe_2 is a paramagnetic heavy fermion with no strong evidence for being close to a ferromagnetic instability [13]. Among the hardest yet most important questions is to understand what could drive such a system toward a spin-triplet superconducting ground state. Having better hints of where to look for or how to build spin-triplet superconductors would be of interest far beyond the community of quantum materials. This work brings unprecedented elements directly related to this issue, supporting notably that magnetic field could drive UTe_2 from a spin-triplet to a spin-singlet ground state.

Up to now, evidence for spin-triplet pairing in UTe_2 has come from NMR Knight-shift measurements, recently performed along all crystallographic axes [14], and from the strong violation of the paramagnetic limit by the superconducting upper critical field H_{c2} [6,11,12,15,16]. The analysis of H_{c2} is, however, not straightforward in UTe_2, because the field-reinforced phase observed for magnetic fields applied along the hard b axis strongly suggests a field-enhanced pairing strength [6,11]. Such a field-dependent pairing is difficult to model theoretically and makes the analysis of H_{c2} more complex, because it opens other routes for a violation of the paramagnetic limit than spin-triplet pairing [13]. Moreover, even the simplest question of whether or not the field-reinforced state has a different symmetry than the low-field one is up to now not settled. Yet experimentally no thermodynamic phase transition had been observed separating low-field and high-field reinforced superconductivity.

Nonetheless, high pressure experiments demonstrate unambiguously that UTe_2 does belong to the very select class of unconventional superconductors displaying transitions between different superconducting phases [17–20]. Some samples even show a double transition at ambient pressure in zero field, which could explain how this low symmetry system (UTe_2 is orthorhombic) could also be chiral. Indeed, the observation of time reversal symmetry breaking below T_c by polar Kerr-effect measurements [21], or the asymmetric spectrum observed with STM spectroscopy [22], suggests such a chiral state. Actually, there is now more and more evidence that the double transition at ambient pressure in zero field is not an intrinsic effect [13,20,23,24].

This rich superconducting state inspired several theoretical works, proposing different scenarios for the possible symmetry states under magnetic field and pressure [8,25,26]. These works also address the deeper question of why this system is spin-triplet. It is particularly acute in UTe_2 because contrary to initial expectations, no ferromagnetic fluctuations have yet been detected. Such magnetic fluctuations, present in the ferromagnetic superconductors [4] and necessary to explain the stability of the A phase of superfluid ^{3}He [2], are natural candidates for the pairing mechanism of spin-triplet superconductors. By contrast in UTe_2, neutron measurements have only revealed incommensurate magnetic fluctuations [15,27,28] and a resonance at finite $\boldsymbol{Q}$ below the superconducting transition temperature T_c [29,30]. UTe_2 could be similar to UPt_3, where neutron scattering studies also mainly detect antiferromagnetic correlations [31]. Therefore, some theories have attempted to explain the observed E_{2u} superconducting ground state of UPt_3 with a pairing mechanism based on pure antiferromagnetic fluctuations [32].

In UTe_2, theoretical models of the spin-triplet superconducting state have explored three main scenarios, starting from band structure calculations: (i) ferromagnetic fluctuations, winning over antiferromagnetic fluctuations for specific values of the normal state parameters (exchange constants, Coulomb repulsion, etc.) [7,26], (ii) local (intra-unit-cell) ferromagnetic correlations between the nearest neighbor uranium ions [25,33], and (iii) pure antiferromagnetic fluctuations, combined with multiorbital degrees of freedom [34] or peculiar conditions on the $\boldsymbol{Q}$-dependent susceptibility and the underlying Fermi surface [35].

Our detailed thermodynamic measurements presented here demonstrate that the field reinforcement of H_{c2} in UTe_2 arises from a new superconducting phase. It is driven by a pairing mechanism different from that controlling the low-field superconducting phase, imposing new constraint on the possible pairing mechanisms. Conversely, we also find that in the low-field phase, pairing is suppressed by magnetic fields applied along the easy magnetization a axis. Altogether, we show that the superconducting symmetry may change from a spin-triplet to a spin-singlet state as a function of magnetic field on approaching the metamagnetic instability transition at $H_m = 34.75$ T for field along the b axis. These new features are solid experimental inputs challenging the theoretical scenarios for the superconducting pairing in UTe_2.

The present paper is organized as follows. In Sec. II, we give a rapid overview of the main experimental results. Section III gives the experimental details. The results are

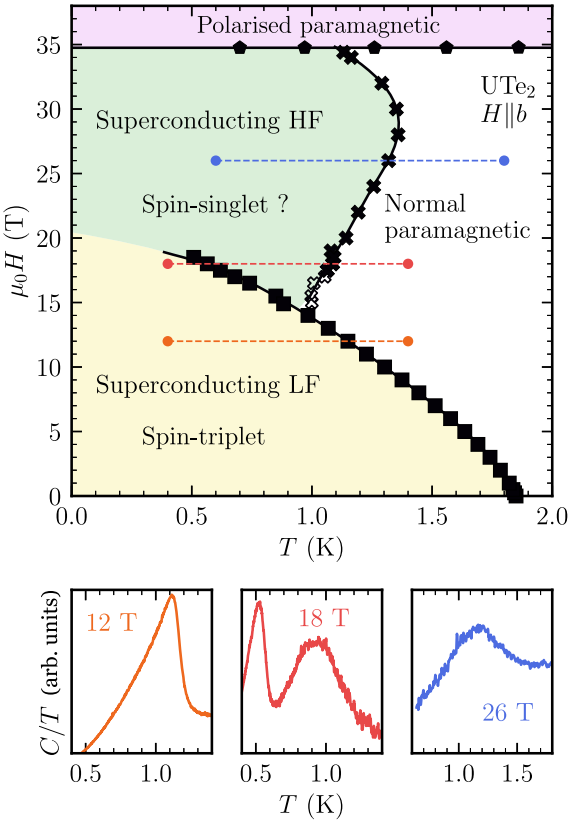

FIG. 1. Top: bulk superconducting phase diagram of UTe_2 for a magnetic field H along the b axis. The specific heat measurements reveal a phase transition line between a low-field (LF) (yellow) and high-field (HF) (green) superconducting state. As a function of magnetic field, superconductivity is suppressed at 34.75 T by a first-order metamagnetic transition marking the entrance in a partly polarized magnetic phase (magenta). Bottom: specific heat divided by temperature as a function of temperature at different magnetic fields. Left: at 12 T a sharp anomaly marks the superconducting transition to the LF phase. Middle: on cooling a broad humplike transition occurs at the transition to the HF phase above a sharp low-temperature transition to the LF superconducting phase. Right: at 26 T only the humplike transition to the HF superconducting phase is observed.

presented in Sec. IV and analyzed in Sec. V. In Sec. VI, we discuss their impact and the open questions. Additional data or details on the methods used for the analysis are reported in Appendixes.

II. OVERVIEW OF THE MAIN RESULTS

This work reveals a thermodynamic phase transition between the low- and high-field reinforced superconducting phases, for magnetic fields applied along the hard magnetization b axis. This has been made possible thanks to specific heat experiments up to 36 T and thermal dilatation or magnetostriction measurements up to 30 T. We also uncover a drastic alteration of the specific heat anomaly along H_{c2} between the two phases, a unique feature, still never observed in any unconventional superconductor, strongly suggesting a change of pairing mechanism between the two superconducting phases.

Figure 1 is a summary of this main result, showing the phase diagram for field along the b axis, with the two superconducting phases (labeled LF and HF for "low field" and "high field," respectively) and the specific heat anomalies at the different phase transitions. Phase transitions between superconducting phases of different symmetries are rare; however, such a change in the specific heat anomaly between the different phases is, to the best of our knowledge, unique. Analysis is required to reveal that it suggests different spin states characterizing these two phases, with a HF phase in strong interplay with the metamagnetic transition occurring at H_m. The result, which is rather counterintuitive, suggests that the LF phase would be spin-triplet, and the HF phase spin-singlet, most likely triggered by the development of antiferromagnetic correlations on approaching H_m. Hence, this would be a direct consequence of the competing pairing interactions (or of the change of dominant finite $\boldsymbol{Q}$ vector in the magnetic excitation spectrum) predicted to occur in UTe_2 [7,26,35].

Another surprise uncovered by these specific heat measurements is that $H_{c2}(T)$ appears to be anomalous not only along the b axis, with the field-reinforced HF phase, but also along the c and most importantly along the easy a axis. This had been completely overlooked up to now, but determination of $H_{c2}(T)$ by specific heat reveals a very strong negative curvature of H_{c2} along the a axis very close to T_c, and an initial slope 4 times larger than initially thought. Hence, a new mechanism is required to explain the very strong deviation of $H_{c2}(T)$ from the linear behavior expected below $T_c/2$ (see Fig. 2): we show that a strong paramagnetic limitation, already excluded by recent NMR Knight-shift measurements [14], would not be sufficient to explain this singular temperature dependence of H_{c2}. Instead, it points to a severe suppression of the pairing strength along the easy axis. In the case of UTe_2, it could arise from at least two different sources. Suppression of (hypothetical) ferromagnetic fluctuations by fields along the easy axis would lead to such a decrease of the pairing strength, a mechanism similar to that in ferromagnetic superconductors [36,37], but also working for paramagnetic systems [38]. Or the strong sensitivity of finite-$\boldsymbol{Q}$ (spin-triplet) pairing [34,35] to Fermi-surface instabilities, already revealed in UTe_2 at rather low magnetic fields along the a axis [39], might also lead to pairing strength suppression.

Hence, both results along the hard b axis and the easy a axis bring new elements on the possible symmetry states in UTe_2 and on the competing pairing mechanisms. It enlightens the stunning superconducting properties of UTe_2, and uncovers key features which should guide future theory developments. Indeed, understanding the mechanisms leading to the strong field dependence of the pairing

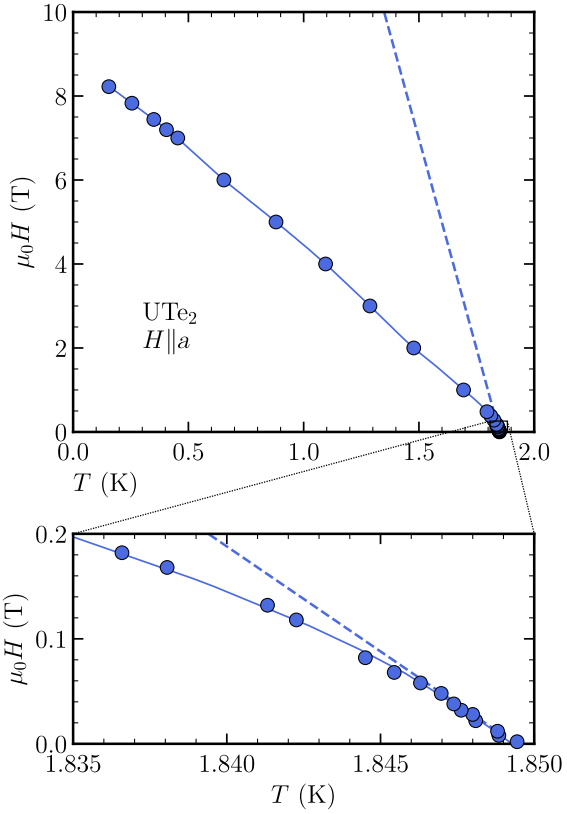

FIG. 2. Top: H_{c2} along the a axis. Dashed line: orbital limit deduced from the measured initial slope at T_c. Bottom: enlargement of the very low field behavior, close to T_c, showing the very strong negative curvature responsible for the deviation of H_{c2} along a from the orbital limitation. This anomalous behavior signs a strong suppression of the pairing strength for fields applied along the easy magnetization axis, an effect also observed in the ferromagnetic superconductors.

strength in UTe_2 is an issue barely touched by current theoretical models, but certainly central for this system and clearly of major interest for the whole field of unconventional superconductivity.

III. EXPERIMENTAL DETAILS

A. Single crystal growth and samples

Different single crystals of UTe_2 from three different batches have been studied by specific heat and magnetostriction or thermal expansion measurements. All single crystals were prepared by the chemical vapor transport method with iodine as transport medium. A starting ratio of U:Te = 2:3 has been used and the quartz ampules have been heated slowly up to a final temperature of 1000 °C on one side and 1060 °C on the other side, and this temperature gradient was maintained for 18 days. The ampules have been slowly cooled down to ambient temperature during 70 h. A sample (no. 1) with a superconducting transition temperature T_c of 1.45 K, a mass of 12.3 mg, from the same batch as those of Refs. [11,40], has been used for the magnetostriction studies. Samples, 2 and 3 with masses of 5.6 mg and 27 μg, respectively, are from another batch with a critical temperature around 1.85 K, and were used for most of the specific heat measurements. Thermal expansion has been measured on a fourth crystal (sample 4), very similar to samples 2 and 3 regarding the specific heat in the normal state, the specific heat jump at $T_c \approx 1.85$ K, as well as the residual value γ_0: we found $\gamma_0 \approx 0.03$ J K^{-2} mol^{-1} at 0.1 K, or 0.011 J K^{-2} mol^{-1} extrapolated toward $T = 0$ from above 0.3 K. Note that the entropy balance at T_c is also well satisfied on these samples (2–4; see Appendix C).

B. Specific heat measurements

The specific heat of two samples (1 and 2) has been measured by a quasiadiabatic relaxation method in a dilution refrigerator up to 15 T in a superconducting magnet and down to 100 mK. Small heat pulses of maximum 1% of the temperature T (0.5% in the superconducting transition) were applied to the samples. The specific heat C is extracted from the temperature response of the sample during the whole pulse sequence. Down to the lowest temperatures, only one relaxation time was measured in the exponential decay. The addenda have been measured separately. They represent 8% of the total measured specific heat at 2 K and 2% at 100 mK. Mainly, temperature sweeps were performed, but also some field sweeps for the transitions at the lowest temperatures (between 100 and 200 mK).

To align the samples in the magnetic field, we used a piezoelectric rotator allowing a rotation over 90° in a plane parallel to the field, and a goniometer allowing a ±3° rotation perpendicular to the plane. Furthermore, the setup is rigid, so that the torque between magnetic field and the anisotropic magnetization of the sample could not induce a misalignment.

Sample 3 (of 27 μg) has been measured with an ac specific heat technique in a ^{3}He refrigerator down to 600 mK, and up to 36 T in the M9 magnet at the high magnetic field laboratory LNCMI in Grenoble. Details of the specific heat setup are shown in the Supplemental Material of Ref. [41]. For fields up to 18.5 T, the ac calorimetry has been performed using a 20 T superconducting magnet (M2) in combination with a ^{3}He refrigerator down to 400 mK. An attocube piezorotator allowed for a rotation in the (b, c) plane.

The value of the critical temperature T_c is extracted from the specific heat transition by a fit to an ideal jump broadened by a Gaussian distribution of critical temperatures: T_c corresponds to the center of this distribution. This model, which reproduces the data very well, allows us to extract directly other parameters like the width and jump of the specific heat at the transition (more details in Appendix E 2).

C. Linear magnetostriction and thermal expansion measurements

The linear magnetostriction $\Delta L_b/L_b$ of UTe_2 has been measured on single crystal 1. In addition, we measured the linear thermal expansion at constant magnetic field on single crystal 4.

These measurements have been performed using a high resolution capacitance dilatometer [42]. The capacitance has been determined using an Andeen Hagerling capacitance bridge AH2550A. High magnetic field experiments have been performed using the 30 T magnet M10 of the high magnetic field laboratory LNCMI Grenoble. Because of the limited diameter of the magnet, it has only been possible to measure the length change ΔL_b parallel to the magnetic field applied along the b axis of the crystal. The magnetic field has been swept with a maximal rate of 100 G/sec to avoid eddy currents heating. The dilatometer was positioned at the end of a silver cold finger in a ^{3}He cryostat, with a base temperature near 370 mK. A RuO_2 thermometer and a heater were fixed directly on the dilatometer. Temperature sweeps at fixed magnetic field have been performed with maximal heating rates of 0.1 K/min.

Additional thermal expansion measurements have been performed in a superconducting magnet up to 13 T using a dilution refrigerator in CEA Grenoble.

IV. RESULTS

A. Magnetic field $H \| b$

1. Specific heat

In zero field, all samples studied exhibit a single sharp superconducting transition (width $\Delta T_c \approx 20$–38 mK), with a large jump at the superconducting transition (up to $\Delta C/C \approx 1.85$), emphasizing the high quality and homogeneity of the samples (see Fig. 3 for sample 2). The specific heat measurements on the first UTe_2 samples displayed an upturn and a large residual term of C/T at low temperatures [43]. Both became smaller with improved sample quality. Our measurements on crystal 2 show indeed only a small residual term, and an upturn shifted to lower temperatures compared to samples with lower T_c (more details are found in Appendix E). This agrees with recent works claiming that residual term and upturn are extrinsic to UTe_2 [13,23,44].

Figure 3 shows C/T as a function of temperature also for several magnetic fields $H \| b$ up to 15 T. Under field, the transition remains sharp with a pronounced jump $\Delta C/T_c$ up to 18.5 T [see Fig. 4(a)], so they are easily followed under field.

Remarkably for $H \| b$, C/T shows two transitions above 15 T: in addition to the marked low-temperature transition, a second wide transition (350 mK width at 18 T) appears above this field [see Fig. 4(a)], and above $H \gtrsim 17$ T, it becomes well detached from the sharp transition. We could

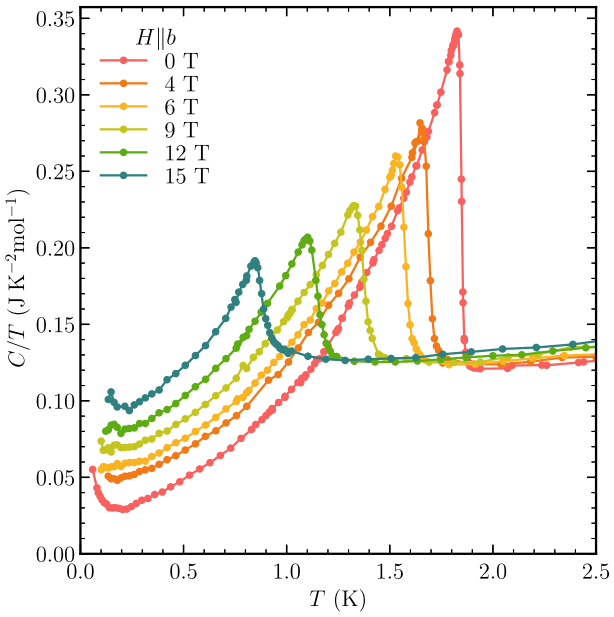

FIG. 3. Temperature dependence of the specific heat C/T at different magnetic fields $H \| b$ from 0 to 15 T measured on sample 2.

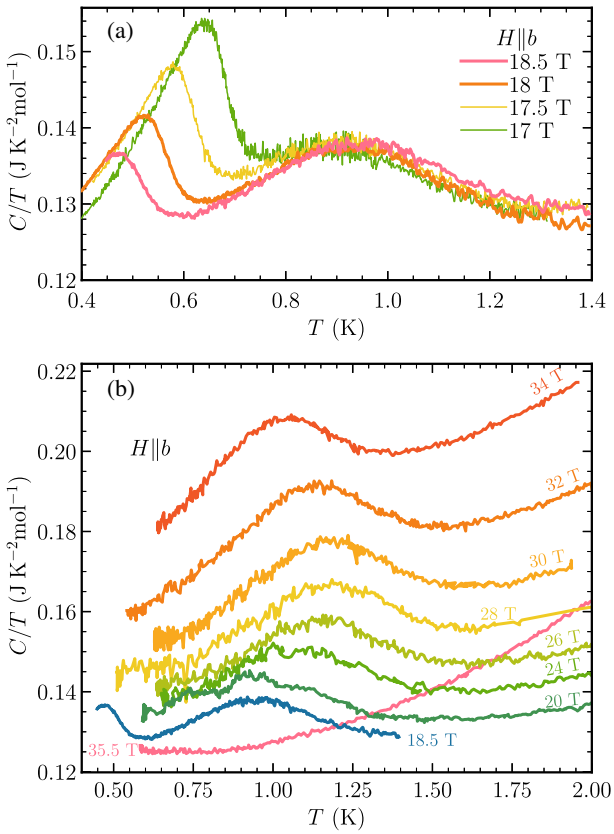

FIG. 4. (a) Temperature dependence of C/T measured on sample 3 for fields $H \| b$ from 17 to 18.5 T. A second wide transition appears above the sharp low-temperature transition. (b) C/T for the different magnetic fields up to 35.5 T, which is above the metamagnetic transition.

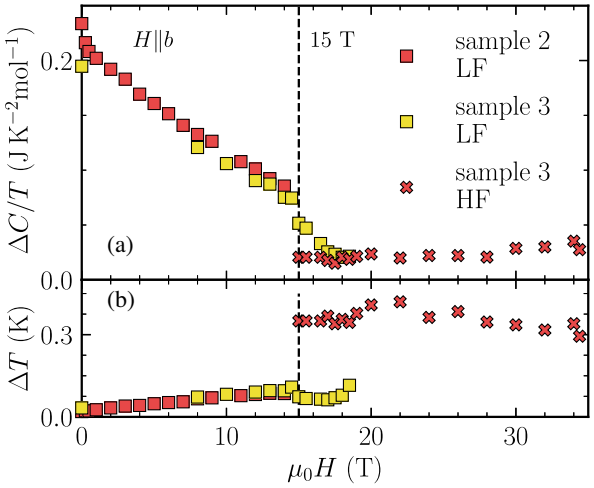

FIG. 5. (a) Jump of the transitions $\Delta C/T_c$ as a function of field, for $H\|b$, determined on samples 2 and 3 for the LF and HF transitions. (b) Width ΔT_c of the transitions as a function of fields. ΔT_c is equal to 2.35 times the standard deviation of the Gaussian distribution of T_c used to fit the transition.

follow this second wide HF transition up to the metamagnetic transition [12,45,46]; see Fig. 4(b).

A Gaussian analysis of the temperature dependence of C/T allows us to deconvolute broadening effects and to determine the jump $\Delta C/T$ at T_c and the width of the transition as a function of magnetic field. They are shown in Fig. 5. The specific heat jump at the transition from the normal to the LF phase decreases with field up to 15 T. When the second broad transition appears above 15 T, the jump at the LF superconducting transition displays a marked drop [see also Fig. 4(a)]. Essentially, it goes down to the same level as that of the wide transition of the normal to HF phase, which remains roughly constant up to H_m. Hence, as expected, the emergence of the HF transition goes along with a redistribution of entropy between both phases.

The T_c of this broad anomaly is increasing with field, except very close to H_m where the transition temperature decreases slightly. This may be due to a slight misalignment of the sample in the high-field experiments or to the torque at the highest field, but it could also be intrinsic. Above H_m, the broad anomaly abruptly disappears. This HF transition is the expected bulk signature of the field-reinforced superconducting phase observed in transport properties for the same field direction [11,12].

Figure 6 displays the field dependence along the b axis of C/T up to 36 T. The sharp LF transition is well observed on these field sweeps. However, the HF transition observed in temperature scans appears here as a very broad and shallow anomaly, noticeable only by comparison with curves at different temperatures. This arises from the combination of an already large T_c distribution at fixed field, with an almost vertical H_{c2}, so that this HF transition

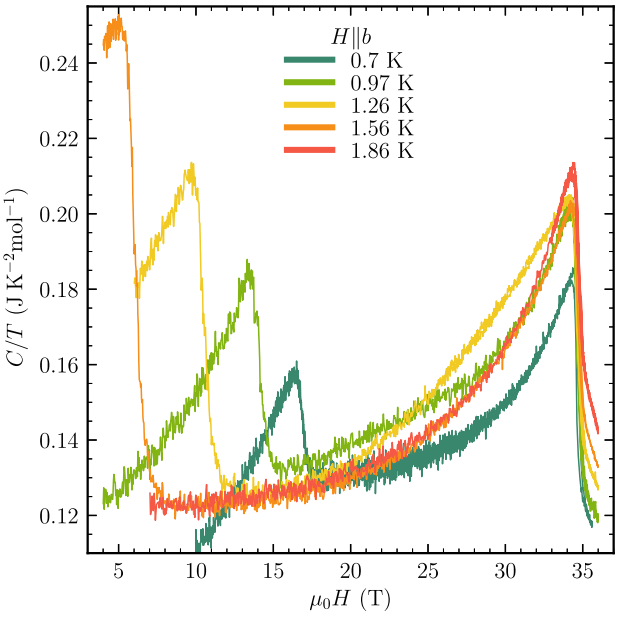

FIG. 6. C/T versus field for $H\|b$ on sample 3 at different temperatures between 0.7 and 1.86 K. The LF superconducting transition and the peak at $H_m = 34.75$ T are clearly visible, but the HF superconducting transition reported in Fig. 4 appears only as a very broad anomaly.

appears extremely broad as a function of field (see Appendix G).

On approaching H_m, C/T shows a strong increase, with a large drop (of order 25%) at the first-order metamagnetic transition, and a hysteresis independent of the sweep rate, displayed in Fig. 7. The drop of the specific heat above H_m is sharpest at the lowest temperature, with a width of 0.25 T. However, a possible interplay between the superconducting and metamagnetic transitions at this temperature may

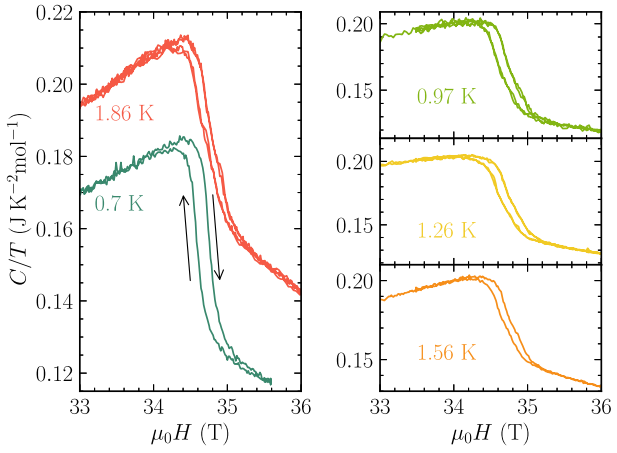

FIG. 7. C/T versus field ($H\|b$) at the metamagnetic transition for sample 3 at different temperatures between 0.7 and 1.86 K. The hysteresis is independent of the field sweep rate. In the left-hand panel, the arrows indicate the direction of the field sweeps.

influence the shape of the anomaly. The width of the hysteresis decreases linearly with increasing temperature, starting from 0.17 T at 0.7 K. This behavior of C/T at H_m agrees qualitatively with previous measurements [47,48] performed in pulsed magnetic fields (see comparison in Appendix D).

2. Complete phase diagram

Since samples 2 and 3 come from the same batch and have essentially the same T_c at 0 T, specific heat measurements on these two samples can be used to establish the complete superconducting phase diagrams for all field directions from 0 to 36 T. It is shown in Fig. 8. As underlined already in Sec. II, a most obvious result is that for $H\|b$, two superconducting phases are clearly present, with a point around $H = 15$ T and $T = 1$ K, where the three transition lines join.

The limits of the LF superconducting phase correspond to the sharp transition that can be followed from 0 T up to 18.5 T. The emergence of the HF phase is revealed by the broad transition appearing above 15 T, and followed up to H_m (Figs. 3 and 4). For magnetic fields slightly above 15 T, the two transitions overlap; thus it is difficult to determine unambiguously T_c for the HF phase transition. Naturally, this also prevents a precise determination of the nature of the crossing of the H_{c2} lines of the LF and HF phases: they could merge with a sharp change of slope, or they could be tangential. Points between 15 and 17 T (empty crosses in Fig. 8) have been determined by fixing the jump height and width of the HF anomaly, using the fact that they both seem to have a negligible field dependence (Fig. 5) (for more details, see Appendix E 2).

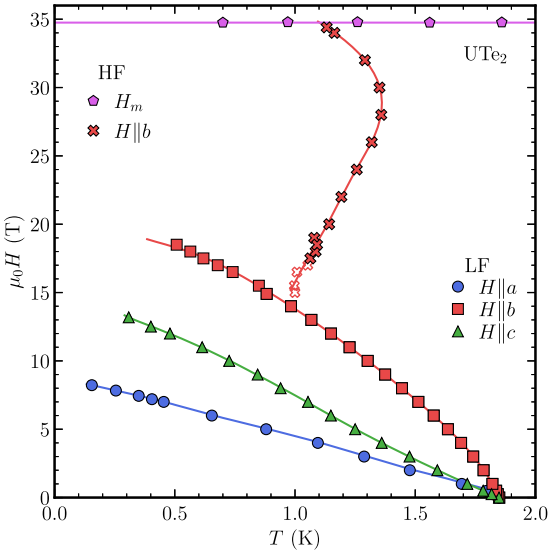

FIG. 8. Phase diagram up to 36 T for H applied along the three crystallographic axes, established with specific measurements on samples 2 (below 15 T) and 3 (above 15 T). Blue circles, $H\|a$; green triangles, $H\|c$; red symbols, $H\|b$. Red squares are T_c from the sharp LF transitions, crosses are T_c from the broad HF transitions. For empty crosses, T_c could only be determined by fixing the width and jump of the HF transition. Magenta hexagons: H_m determined on sample 3 by specific heat from the field up sweeps.

We also found no sign of a fourth transition line inside the LF phase, either on temperature or field sweeps, as would be expected for a crossing of second-order phase transitions [17,49]. However, this absence of a fourth line could also arise from a further broadening of the HF transition inside the LF phase (for fields below 15 T).

Nevertheless, the phase diagram clearly demonstrates the existence of at least two different superconducting phases for $H\|b$: comparison with the resistivity measurements and the observation of vortex pinning in the HF phase by linear magnetostriction (see next paragraph) show that it is also a superconducting phase.

3. Linear magnetostriction

The longitudinal linear magnetostriction $\Delta L_b(H)/L_b$ along the b axis for $H\|b$ of sample 1 is shown in Fig. 9. In the normal state ($T = 2$ K), the linear magnetostriction is negative and shows roughly a H^2 field dependence, as usually observed in paramagnetic metals [Fig. 9(a)]. This is in agreement with the low-field measurements of Ref. [20] and with the very recent measurements in pulsed magnetic fields, which show a strong negative jump of the linear magnetostriction at the metamagnetic transition [50]. Following Maxwell's relations, the negative sign of $\Delta L_b/L_b$ indicates that under uniaxial stress applied along the b axis, the susceptibility χ_b along this axis should increase, as observed under hydrostatic pressure [51].

In the superconducting state at $T = 0.35$ K, the linear magnetostriction shows a very pronounced hysteretic behavior. In Fig. 9(b) we display the additional contribution to the linear magnetostriction ΔL_b^s which appears in the superconducting state. It is obtained from the measured linear magnetostriction at fixed temperature in the superconducting state after subtraction of the paramagnetic contribution measured at 2 K. The linear magnetostriction in the superconducting state is very large and shows a strong hysteresis with a fishtail-like behavior both below ≈15 T and above ≈20 T.

This irreversible magnetostriction appears very similar to the behavior of the magnetization in the mixed state of type II superconductors with strong vortex pinning. Indeed, in the critical state model [52], magnetic flux penetration or expulsion, when increasing (or decreasing) the field, is impeded by vortex pinning. If magnetic flux lines are trapped by the action of pinning forces, equal but opposite forces will act on the lattice, with possible effects on the magnetostriction [53].

At the lowest temperature, the hysteresis in the linear magnetostriction vanishes above $H_{\mathrm{irr},1} \approx 14.5$ T, and it opens again above $H_{\mathrm{irr},2} \approx 21$ T, being maximal at 30 T,

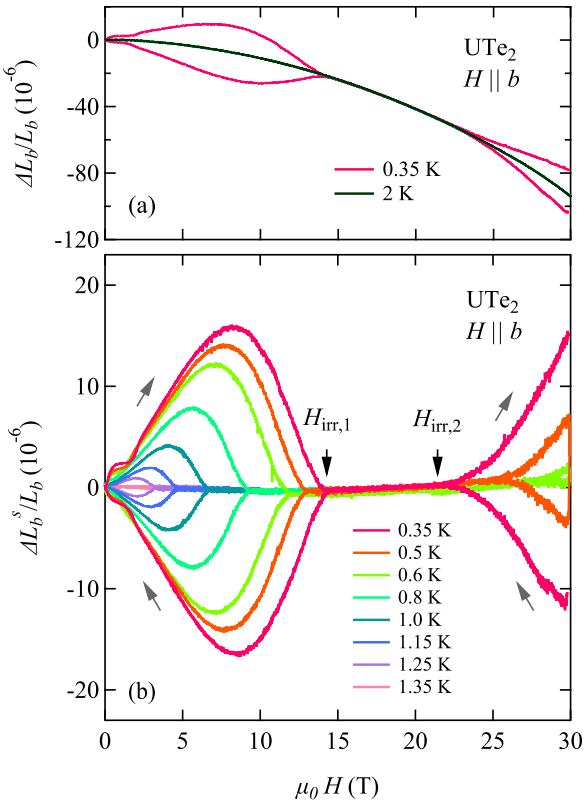

FIG. 9. (a) Longitudinal linear magnetostriction $\Delta L_b/L_b$ of sample 1 along the b axis for a field applied along the b axis, in the superconducting state at 0.35 K and in the paramagnetic state at 2 K. (b) Linear magnetostriction in the superconducting state at different temperatures after subtraction of the paramagnetic contribution measured at 2 K. The gray arrows indicate the direction of the field sweep. Black vertical arrows mark the closing and reopening of the hysteresis as a function of field, which corresponds to the irreversibility field $H_{\rm irr}$ of the vortex motion in the superconductor.

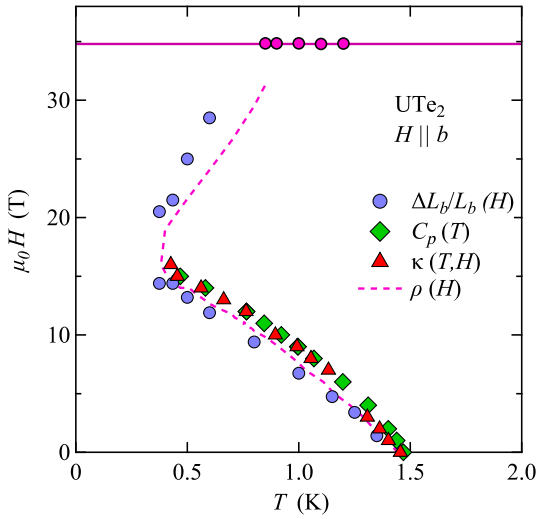

FIG. 10. Phase diagram magnetic field versus temperature for field $H\|b$ for sample 1 with a T_c of 1.45 K. Blue circles, irreversibility fields determined from the magnetostriction measurements (see Fig. 9); green diamonds, H_{c2} from specific heat measurements performed on the same sample; red triangles, H_{c2} from thermal conductivity on a sample from the same batch (Appendix A), and dashed line, H_{c2} determined from the resistivity $\rho(H)$ of another sample from the same batch (data from Ref. [11]). Magenta line: H_m determined from resistivity (circles, Ref. [11]).

which is the highest field we could reach in the experiment. On warming, the lower field $H_{\rm irr,1}$ decreases, while the upper field $H_{\rm irr,2}$ increases, and above 0.6 K, it exceeds the achievable field range. These irreversibility fields are displayed in Fig. 10 and compared with H_{c2} determined from specific heat measurements (only below 15 T on this sample), with thermal conductivity measurements (Appendix A), and also with resistivity measurements on a sample from the same batch with similar T_c (see Ref. [11]).

In the LF phase, thermodynamic as well as thermal and electrical measurements are in good agreement, with only small quantitative differences on the amplitude of the negative curvature of $H_{c2}(T)$ in the 0–5 T field range. Obviously, flux pinning in the sample at low magnetic fields is rather strong, as found by low-field–low-temperature magnetization measurements [54], and the irreversibility field follows the upper critical field: $H_{\rm irr,1} \sim H_{c2}$. In the field-reinforced HF superconducting phase above 15 T, the difference between $H_{\rm irr,2}$ and H_{c2} is much more pronounced: there is a broader reversible regime, between H_{c2} and $H_{\rm irr,2}$, suggesting a decrease of the pinning strength in this phase. Actually, the observation of the irreversible magnetostriction due to the flux pinning between 20 and 30 T is a further proof that the HF phase delimited by the broad specific heat anomaly is indeed a bulk, field-reinforced superconducting phase.

In Appendix B, we also show the linear thermal expansion $\Delta L_b(T)/L_b$ as a function of temperature measured on sample 4, which has a $T_c = 1.82$ K similar to that of samples 2 and 3 studied by specific heat. It confirms the difference of pinning strength between both phases.

B. H_{c2} close to T_c, along all directions

Figure 8 also shows the upper critical field H_{c2} of sample 2 along the a and c axes. Similar to the previous reports [6,11], H_{c2} is strongly anisotropic and extrapolates to 9 T for the a axis and 15 T for the c axis. A more detailed examination reveals that H_{c2} in UTe_2 present anomalies not only due to the presence of the two superconducting phases for $H\|b$: it also has an anomalous temperature dependence for all field directions. The most striking feature appears along the a axis. Over a large temperature range $H_{c2}(T)$ along the a axis appears linear. However, a closer look very near T_c yields a contrasted view, showing that contrary to field directions $H\|b$ and $H\|c$, this linear behavior would extrapolate to a critical temperature 36 mK larger than the

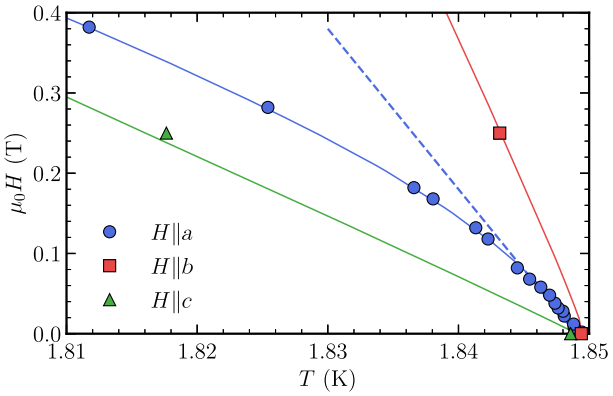

FIG. 11. H_{c2} as a function of temperature determined from specific heat measurements on sample 2 for the three axes at very low fields, close to T_c. Error bars on the determination of transition temperature deduced from the Gaussian analysis of the specific heat anomaly are smaller than the size of the points. The dashed line is a linear fit following the initial slope of H_{c2} along the easy magnetization a axis. It is close to the value along the b axis, however, followed by a very strong negative curvature showing up at very low fields [0.4 T is about $\mu_0 H_{c2}(0)/20$ for $H\|a$].

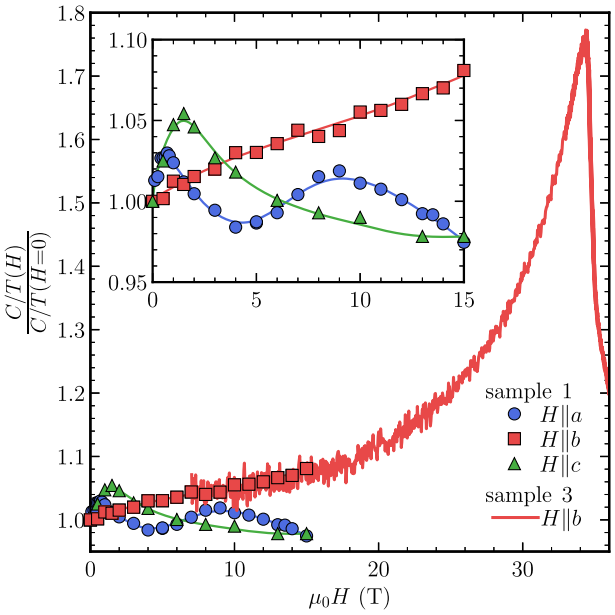

FIG. 12. C/T normalized by its value at zero field, as a function of field for H along a, b, and c axes at 1.86 K. Measurements below 15 T have been done on sample 1, by temperature sweeps. Measurements for $H\|b$ above 15 T have been done on sample 3 by a field sweep at 1.86 K. Inset: enlargement of the measurements below 15 T; lines are guides to the eyes.

experimental value. It can be visualized in Fig. 11, showing the very low field region ($H < 0.4$ T) on an enlarged scale. H_{c2} along the easy a axis displays a very strong negative curvature very near T_c, following an initial slope of order -20 T/K, much larger than anticipated by the "large-scale" linear behavior. It is also much larger than the values determined previously by resistivity measurements: around -5 or -6 T/K depending on the samples [6,10].

Actually, this effect was already present in Ref. [55] reporting also specific heat measurements, but was barely discussed. We have confirmed this anomalous behavior (the very large slope followed by a very strong curvature), on three different samples measured also by specific heat (see Appendix F). Discussion of the possible origin of this very strong curvature along the a axis in UTe_2 is of course central for the question of the symmetry state of the superconducting order parameter in UTe_2 and of the pairing mechanism (see Sec. V A).

For the other directions, there are no anomalies close to T_c. The initial slope has its largest value for $H\|b$: from our specific heat measurements, we determine $dH_{c2}/dT_c \approx -34$ T/K, which is larger than the values obtained from electrical transport measurements: $dH_{c2}/dT_c \approx -25$ T/K [56]. This initial slope is lowest along the c axis: $dH_{c2}/dT_c \approx -7.5$ T/K, and $H_{c2}(T)$ along this axis displays an usually large linear regime from T_c down to 0.5 K.

C. Normal phase specific heat

The very large specific heat jump at T_c clearly indicates that UTe_2 is in a strong-coupling regime. The most natural explanation for the field-reinforced superconducting phase is that the superconducting pairing itself is enhanced under fields along the b axis [6,11]. As discussed already for the ferromagnetic superconductors, in the strong-coupling regime, such a field dependence should be reflected also in the normal state Sommerfeld specific heat coefficient γ [37,57]. In UTe_2, it is not easy to determine the Sommerfeld coefficient, because C/T remains strongly temperature dependent almost down to T_c, and there is no simple way to analyze this temperature dependence (see Appendix C). This arises mainly from a marked anomaly in the specific heat with a maximum at a temperature $T^* \approx 12$ K, attributed to magnetic fluctuations [58].

We show in Fig. 12 $C(H)/T$ normalized to C/T in zero field, at $T = 1.86$ K for fields applied along the three crystallographic directions. As the temperature dependence of C/T becomes weak at this temperature, it can be considered as a reasonable estimation of the γ value, at least as long as the applied field is not too close to H_m. Indeed, the specific heat anomaly at 12 K is shifted to much lower temperatures on approaching H_m for $H\|b$ [13,58]. Hence, for this field direction, magnetic fluctuations are likely to contribute to the large enhancement of C/T close to H_m, clearly visible in Fig. 12. The subsequent sharp drop of C/T above H_m might arise from the Fermi surface instability detected at the metamagnetic transition [59] and/or from a suppression of magnetic fluctuations in the polarized phase.

These results for $H\|b$ are similar to already published data [46–48], with some quantitative differences notably above H_m, where the ac technique in static fields probably allows for more precision. For field along the a or c axis, $C/T(H)$ has an even more complex behavior. It is known that along the a axis Lifshitz anomalies appear around 5 T and possibly 9 T [39]. They do appear as extrema of C/T on our measurements (temperature dependence in Appendix C). In addition, we also observe pronounced maxima of C/T along the a and c axes at low field, respectively, at 0.5 and 1.5 T, whose origin is still unclear. Until better understood, it is difficult to rely on the field dependence of C/T in the normal phase to discuss quantitatively the behavior of the pairing strength with field.

V. ANALYSIS

A. H_{c2} in the LF phase

We first discuss the behavior of H_{c2} close to T_c. Indeed, the observed negative curvature of H_{c2} along the a axis suggesting a severe paramagnetic limitation might seem to contradict the common belief that UTe_2 is a p-wave superconductor with a $\boldsymbol{d}$ vector perpendicular to the easy a axis.

Such a paramagnetic limitation would be at odds with the value of $H_{c2}(0) \sim 9$ T, which is much larger than the weak-coupling paramagnetic limit of around 3.5 T (for a gyromagnetic factor $g = 2$ with $T_c = 1.85$ K). Actually, the negative curvature is so concentrated close to T_c that it requires a very large value of g ($g \approx 3.2$ in the weak-coupling limit, so even larger in the strong-coupling regime) to match the initial deviation from linearity of H_{c2} along the a axis, leading to a saturation of $H_{c2}(0)$ at 2.25 T at low temperatures [see Fig. 25(b) in Appendix J]. In other words, $H_{c2}(T)$ along the easy axis does not follow at all the temperature dependence of an upper critical field solely controlled by paramagnetic and orbital limitations [60]: paramagnetic limitation is not a satisfying explanation for the strong negative curvature close to T_c.

Nonetheless, the large value of the initial slope dH_{c2}/dT_c along the a axis obtained when taking account of this strong curvature (Fig. 11) is in excellent agreement with the initial slope $dH_{c2}/dT = -20.4$ T/K determined from the lower critical field H_{c1} and the thermodynamic critical field H_c (for details, see Appendix H and Ref. [54]). From the resistivity measurements which essentially extrapolate the linear regime up to T_c, a much smaller value (around -8 T/K) is found, which contradicts the relation with H_{c1} and the critical thermodynamic field. So, this agreement between the large value of the dH_{c2}/dT_c and the measurement of H_{c1} supports the intrinsic character of the strong curvature of H_{c2} close to T_c for H along the a axis.

Before examining more quantitatively a possible explanation for this curvature, it is worth analyzing the situation along the c and b axes.

Regarding the same comparison of H_{c1} with H_{c2} along the c axis, the agreement is also very good: from the values of dH_{c1}/dT_c along the c axis in Ref. [54], we expect a value of dH_{c2}/dT_c of -7.6 T/K, again in excellent agreement with the present determination of -7.5 T/K. This contrasts with the case for $H\|b$. As stated already in Ref. [54], the anisotropy of H_{c1} between the b and c axes at T_c is very small. Hence, dH_{c2}/dT_c should be roughly equal (and of the order of -8 T/K) in both directions, whereas the present experiment yields $dH_{c2}/dT_c = -34$ T/K along the b axis. In addition, the temperature dependence of H_{c2} along the c axis and the b axis further away from T_c also cannot be reproduced by any combination of paramagnetic and orbital limitation (see Appendix J).

The most direct way to explain these anomalies regarding the value of the slope at T_c (for $H\|b$) and the temperature dependence of H_{c2} along all directions and notably for $H\|a$ is a field-dependent pairing strength. This happens also in ferromagnetic superconductors [37] and has been already proposed for $H\|b$ in UTe_2 [6,11]. If we call λ the strong-coupling parameter controlling this pairing strength, it has to be field dependent in all directions. We can rely on H_{c1}, which is small enough for the effects of such a field dependence to have negligible impact [54], to fix the average Fermi velocities controlling dH_{c2}/dT_c for $H\|b$, without the contribution of the field-dependent pairing strength. Along the a and c axes, the agreement between dH_{c1}/dT_c and dH_{c2}/dT_c shows that $[d\lambda(H)/dH] \approx 0$ in zero field (at T_c).

For the estimation of $\lambda(H)$ in the different field directions, there are general constraints which are model independent. First of all, along the b axis, the discrepancy between dH_{c1}/dT_c and dH_{c2}/dT_c can only be reconciled with an increase of the pairing strength: increasing dH_{c2}/dT_c requires $[d\lambda(H)/dH](H = 0) > 0$. Hence, we expect an increase $\lambda(H)$ along the b axis not only in the HF phase, but also in the LF phase.

For $H\|c$, starting with $[d\lambda(H)/dH](0) = 0$, the small positive curvature and the very linear behavior also require an increase of $\lambda(H)$, whatever the strong-coupling model and the mechanisms (orbital and/or not paramagnetic limitation).

The situation is not as straightforward for $H\|a$; however, the most natural explanation is that the deviation from linearity observed very close to T_c arises from a strong suppression of $\lambda(H)$, with an H_{c2} otherwise purely orbitally limited (details are in Appendix J). This scenario is consistent with the NMR results, yielding essentially no change of the Knight shift at T_c along the a axis [14].

Following theses NMR results we also assume a negligible paramagnetic limitation in the (LF) phase along the b and c axes. The superconducting order parameter symmetry has an impact on the value of the initial slope dH_{c2}/dT_c, but influences little the temperature dependence of H_{c2} due to the orbital limitation. Hence, we can use

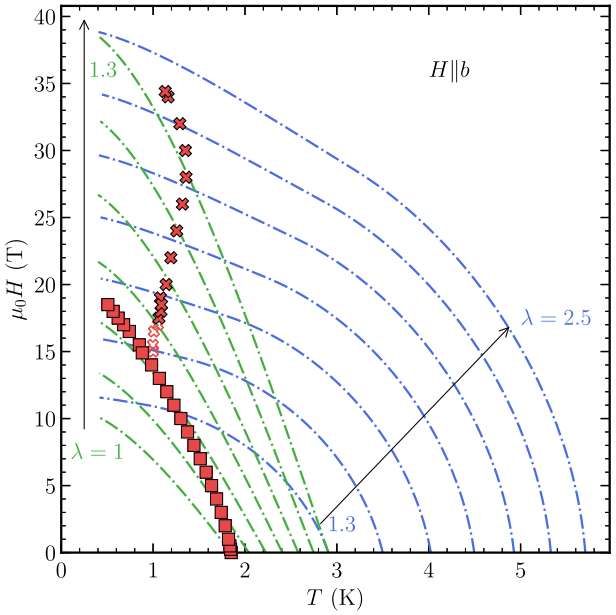

FIG. 13. Crosses and squares are data of H_{c2} for $H\|b$. Dashed lines are the H_{c2} calculated for different fixed values of the coupling constant λ. The green lines correspond to calculation for $g = 0$ by steps of $\Delta\lambda = 0.05$, and the blue lines for $g = 2$ by steps of $\Delta\lambda = 0.2$.

the same strong-coupling model as in Refs. [11,37], which mimics H_{c2} for a spin-triplet superconductor with a calculation for an s-wave superconductor without paramagnetic limitation (taking $g = 0$ in the equations). Averaged Fermi velocities for the different field directions have been chosen so that the initial slopes dH_{c2}/dT_c for a field-independent pairing strength have the values calculated from dH_{c1}/dT_c (see Table I in Appendix H).

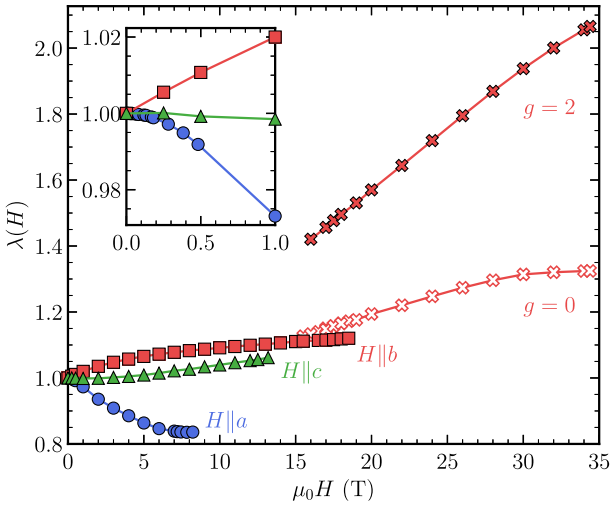

FIG. 14. $\lambda(H)$ determined from H_{c2} along three crystallographic axes, measured on sample 2. λ was set to 1 at 0 T, g to 0 for the LF phase. For the HF phase, plain red crosses are $\lambda(H)$ determined with $g = 2$, and empty red crosses are $\lambda(H)$ without paramagnetic limit ($g = 0$). An enlargement of fields below 1 T is shown in the inset.

The different calculations of H_{c2} for $H\|b$ with the two hypotheses, spin-triplet superconductivity with no paramagnetic limitation and spin-singlet with full paramagnetic limit at constant pairing strength, are presented in Fig. 13. The large enhancement of the paramagnetic limit due to the correlated increase of the pairing strength λ and the corresponding critical temperature in zero field is clearly visible. The deduced field dependence of the pairing strength $\lambda(H)$ is reported in Fig. 14 for the three crystallographic directions and the two models for $H\|b$. Fit parameters are reported in Table II in Appendix J, and the model is described in Appendix I.

The increase of λ along the c and even b axes is modest in the (LF) phase, at most 10%, whereas a strong suppression is required for $H\|a$. The inset of Fig. 14 shows that despite the strong suppression of the pairing for $H\|a$, in zero field $(d\lambda/dH) = 0$. This originates directly from our choice of matching the initial slope dH_{c2}/dT_c at constant λ with the values deduced from H_{c1}.

B. H_{c2} in the HF phase

Theoretical models for the HF phase have proposed a field-induced symmetry change of the order parameter [8,25]. The main idea is that for a spin-triplet superconducting state arising from ferromagnetic fluctuations along the easy magnetization axis, at low fields, the $\boldsymbol{d}$ vector should be perpendicular to the a axis. Hence a B_{3u} (or more generally $B_{3u} + iB_{1u}$ state under field [13]) is favored at low fields. By contrast, for strong fields along the b axis, a rotation of the $\boldsymbol{d}$ vector is expected toward a B_{2u} state (or $B_{2u} + iA_u$), to minimize the component of the $\boldsymbol{d}$ vector along the b axis. Such a symmetry change would imply a phase transition somewhere between the low- and high-field regimes, which had not been detected until the present specific heat measurements. Nonetheless, this change of $\boldsymbol{d}$ vector orientation alone could only explain that an initial paramagnetic limitation is exceeded thanks to the new orientation of the $\boldsymbol{d}$ vector. It will not explain the positive dH_{c2}/dT observed in the HF phase between 15 and 30 T.

Conversely, empirical explanations of the reinforcement of H_{c2} focused on field-induced enhancement of the pairing (positive $d\lambda = dH$) [6,11]. This pairing enhancement could originate from an additional field-induced phase transition. However, in the previous studies [6,11] this enhancement as obtained from the analysis of the reinforcement of H_{c2} did not imply such a phase transition. Indeed, even the rather sharp upturns observed on H_{c2} extracted from electrical transport could be reproduced with a smooth continuous increase of $\lambda(H)$ [13].

The present detailed specific heat measurements demonstrate not only that there is a field-induced thermodynamic phase transition between two different superconducting

states, but also that the pairing mechanisms driving these phases are likely different. This is first seen from the phase diagram of Fig. 8, where the appearance of the HF phase appears very abruptly, marked by a sharp increase of $T_c(H)$ contrasting with the smooth continuation of the LF phase. In addition, the specific heat anomaly for both phases is markedly different, with a very broad anomaly in the HF phase whereas that of the LF phase remains remarkably sharp (see Fig. 4). Both features differ strongly from the case of UPt_3 [61] or more recently of $CeRh_2As_2$ [62,63], where $T_c(H)$ is always decreasing with field, and no change is observed on the shape of the specific heat transition along H_{c2} when switching from the low- to the high-field superconducting phases.

In UTe_2, there is clearly more than just a rotation of the $\boldsymbol{d}$ vector between the LF and HF phases. Most likely, pairing is reinforced at high fields thanks to the emergence of a new pairing mechanism driven by the proximity to H_m. Unfortunately, the nature of the magnetic fluctuations driving the metamagnetic transition is still unclear (see Appendix D). However, the phase diagram for $H\|b$ under pressure [64] shows that the HF phase could well be the same as the pressure-induced higher T_c superconducting phase [17–20,65]. There are two main theoretical proposals for this "high-T_c" pressure-induced phase. The first [25] is that it is a B_{2u} phase, having no component of the $\boldsymbol{d}$ vector along the b axis, with a pairing mechanism controlled by local ferromagnetic correlations. The second is that it is a spin-singlet (A_g) phase [26], induced by antiferromagnetic correlations becoming dominant over ferromagnetic fluctuations under pressure.

The first proposal is the most natural one, explaining the different phases with a single pairing mechanism and transitions imposed by the Zeeman coupling of the $\boldsymbol{d}$ vector with the applied field. In this framework, nothing should be changed to the procedure for the evaluation of the field-dependent pairing strength $\lambda(H)$ between the LF and HF phases. The result is reported also in Fig. 14 (open red crosses), displaying a cusp at ∼15 T, but a rather weak increase (30% between zero field and H_m) of the pairing strength, far from the factor ≈2 observed on C/T at 1.8 K (Fig. 12).

Using the second proposal of a spin-singlet superconducting order parameter for the HF phase seems paradoxical at first glance, but yields interesting results. Once again, with a field-dependent pairing, the weak-coupling paramagnetic limit is easily exceeded thanks to the effective increase of the "zero-field" T_c and to strong-coupling effects: the ratio $[H_{c2}(0)/T_c]$ increases to a value of ≈4 for $\lambda = 1$, and exceeds 6 for $\lambda = 2$ (see Fig. 13).

This explains how a spin-singlet state could survive at 36 T with a paramagnetic limitation set by a value $g = 2$ of the gyromagnetic factor. Under pressure, this spin-singlet phase can explain the strong paramagnetic limitation observed along the a axis [11,19]. Here, it leads to a larger field dependence of the pairing strength (plain red crosses in Fig. 14), required to overcome the saturation of H_{c2} (at fixed λ) due to the paramagnetic limitation. Estimation of $\lambda(H)$ has been done for a gyromagnetic factor of 2, and (arbitrarily) with the same energy scale Ω as for the LF phase, considering that both mechanisms should have similar characteristics in order to lead to similar critical temperatures. Using different values of Ω (but the same g factor) changes little to the following analysis.

Up to now, we have shown that the spin-singlet scenario for the HF phase is not unreasonable, requiring an increase of the pairing strength (from 1 to 2) which is compatible with the strong increase of electronic correlations observed on approaching H_m as suggested by the strong enhancement of C/T in this field range. It is also in line with the change of pairing mechanisms between the LF and HF phases, supported by the difference in their respective specific heat anomalies, and by the marked positive value of dH_{c2}/dT in the HF phase. We can however go a step further, showing that the spin-singlet state helps in understanding quantitatively the change of the specific heat anomaly.

Indeed, with the field-reinforced pairing the temperature of the superconducting transition in the HF phase depends on the applied field both through the usual orbital and possibly paramagnetic effects and due to the field dependence of the pairing strength: $T_c = T_c[H, \lambda(H)]$. So additional broadening of the superconducting transition may come from a field-dependent dispersion of λ. In the very likely hypothesis where the field increase of the pairing arises from the proximity to H_m, a simple hypothesis is that λ is a function of H/H_m.

Then, a dispersion of H_m controlling the broadened specific heat anomaly reported in Fig. 7 for the metamagnetic transition will translate into a distribution of T_c, hence to a new mechanism for the broadening of the superconducting transition. From the calculation of H_{c2} at fixed λ used to extract the field dependence of the pairing, we can determine $T_c = \varphi[H, \lambda(H/H_m)]$. This allows us to determine the effect of the distribution of H_m on the specific heat anomalies of the HF phase according to the two different determinations of $\lambda(H)$.

With this hypothesis in the spin-singlet case, the measured dispersion of H_m of order 0.55% explains half the width of the superconducting transition. As shown in Fig. 15, the observed anomaly is well fitted all along the H_{c2} line of the HF phase by doubling the measured H_m dispersion. By contrast, it fails completely in the spin-triplet case. A simple analysis (see Appendix K) reveals that the key advantage of the spin-singlet scenario is the much larger value of $(\partial T_c/\partial H)|_\lambda$ imposed by the paramagnetic limitation. Within this scheme, the dispersion of H_m is found to have a negligible influence on the LF transition, so that it does give a first explanation for why the two superconducting phases could be marked by such different specific heat anomalies.

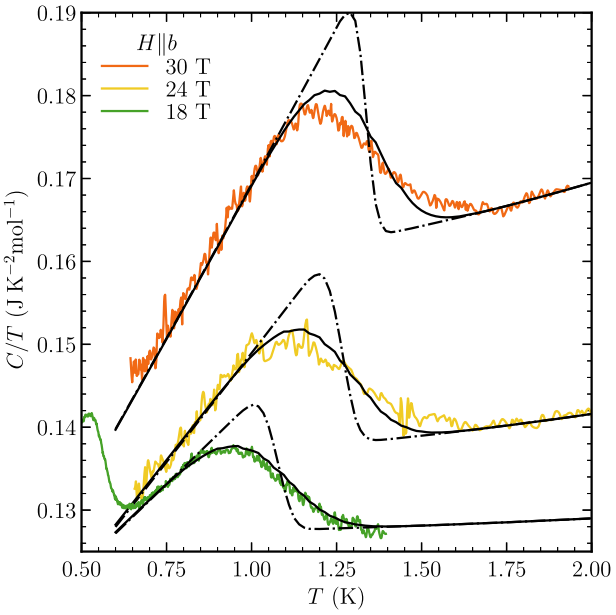

FIG. 15. The HF transition at 18, 24, and 30 T, $H\|b$, measured by specific heat. Data (color) and fits (black lines) of the specific heat anomalies calculated for the spin-singlet ($g = 2$, continuous line) or spin-triplet ($g = 0$, dash-dotted line) superconducting state in the HF phase. The broadening in the fits arises from the measured distribution of H_m, however, multiplied by a factor 2.3. For the spin-triplet state, even with a distribution of H_m twice larger than given by our measurement, we fail to reproduce the broadening. By contrast, for the same larger distribution of H_m, the agreement is good for the spin-singlet scenario.

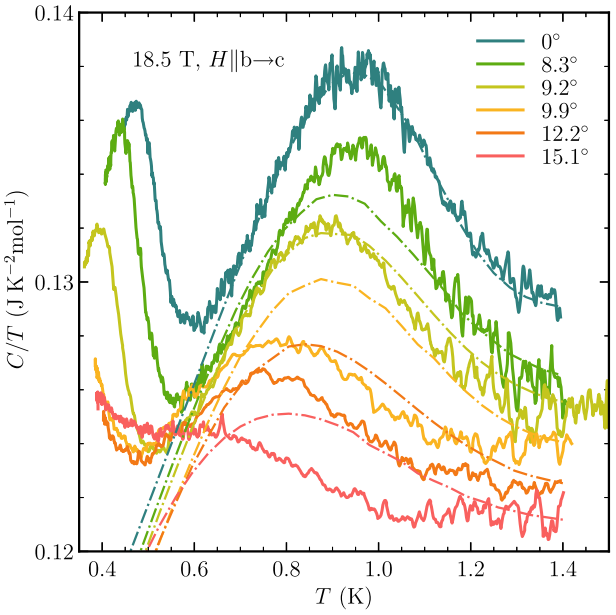

FIG. 16. Temperature dependence of C/T measured on sample 3 at 18.5 T for different angles in the (b, c) plane. Dash-dotted lines are the transitions calculated from a distribution of H_m, controlled by its angular dependence [12] and a finite mosaicity of 3° in the sample.

Moreover, when the sample is misaligned in the (b, c) plane the transition shifts to lower temperatures and the amplitude of the jump decreases; see Fig. 16 for an applied field of 18.5 T (more data in Appendix L). At 15° the HF transition almost disappears. Taking into account only the angular dependence of H_m [12], and a hypothetical mosaicity of 3° in our crystal, we can roughly reproduce the huge broadening of the anomaly at finite angles, with the same dependence of T_c on H_m (dash-dotted lines in Fig. 16), and otherwise a constant ideal specific heat jump. This is another support for this explanation of the large broadening of the specific heat anomaly relying on the spin-singlet scenario.

VI. PERSPECTIVES

A main result from this work is the requirement of a field-dependent pairing strength along all directions of the applied field, as shown by the anomalous temperature dependence of H_{c2} along the a, b, and c axes already close to T_c. The strong decrease of the pairing strength along the a axis is reminiscent of the results on UCoGe along its easy magnetization axis, and at first sight, it seems best compatible with a pairing mechanism involving true ferromagnetic fluctuations. Even subtle differences between the two systems are explained by such a mechanism. For example, in UCoGe, the slope of H_{c2} along the easy axis is strongly suppressed already at T_c, showing that $d\lambda/dH$ is large and negative. In UTe_2 for $H\|a$, comparison of H_{c2} and H_{c1} showed that $(d\lambda/dH) \approx 0$. This is consistent with the predictions for ferromagnetic and paramagnetic superconductors, respectively, where $d\lambda/dH$ due to the suppression of "ferromagnetic" fluctuations is proportional to $M_z(\partial M_z/\partial H)$ (M_z being the magnetization along the easy axis) [38]. So $d\lambda/dH$ at T_c ($H = 0$) should be zero in paramagnetic systems (like UTe_2), and nonzero in ferromagnets below the Curie temperature, as long as the magnetization is not completely saturated.

There are also several theoretical studies exploring other mechanisms leading also to spin-triplet pairing, like finite momentum magnetic fluctuations [35], or only local ferromagnetic correlations within a unit cell [25]. The field dependence of such mechanisms has not been explored. However, the Fermi-surface instability observed at 6 T along the easy axis [39] could play a key role if $\boldsymbol{Q}$-dependent pairing is important. Hence, even though ferromagnetic fluctuations are a likely mechanism for the LF phase of UTe_2, we cannot exclude that future investigations of these alternative mechanisms could also yield satisfying explanations of the present measurements.

Concerning the results along the hard b axis, the pertinence of the comparison of UTe_2 with the ferromagnetic superconductors becomes more suspicious. For this field direction, the main result is the existence of two different bulk superconducting phases already at ambient pressure.

Recently, we became aware of a new work on high-field NMR, recovering a similar phase diagram as reported here, but identifying the HF phase as a spin-triplet $A_u + iB_{2u}$ state [66]. This arises from Knight-shift measurements in the HF phase, showing no detectable changes across T_c. We note that due to the field dependence of the pairing strength, these measurements in the HF phase are all performed at values of $H/H_{c2}^{\mathrm{eff}}(0)$ close to 1, where $H_{c2}^{\mathrm{eff}}(0)$ is the effective value of $H_{c2}(0)$, corresponding to the value of the pairing strength $\lambda(H)$ at the field H of the measurement (see Fig. 13). At these large field values [with respect to $H_{c2}^{\mathrm{eff}}(0)$], there is little change to expect for the Knight shift, whatever the spin state.

More recently, a similar phase diagram was also reported from resistivity and ac susceptibility measurements [67]. However, the anomalies revealing the transitions in both of these works could not be used to track the broadening of the transition in the HF phase as revealed by our specific heat measurements. This change of the specific heat anomaly is a unique case showing that this new superconducting phase does not arise from a simple change of symmetry like in UPt_3, or from a rotation of the $\boldsymbol{d}$ vector: it has to arise from a new pairing mechanism strongly reinforced on approaching H_m. We have found support for a paramagnetically limited H_{c2} in the HF phase, hence for a spin-singlet superconducting phase, as it can explain a large part of the strong broadening of the specific heat anomaly in the HF phase, and the still increased broadening when turning away from the b axis in the (b, c) plane.

We also became aware of a theoretical work proposing an alternate explanation for the phase diagram of UTe_2, without field-reinforced pairing [68]: admitting the existence of a transition line between a LF and HF superconducting phase, the "deep" of H_{c2} at 15 T would be caused by thermal superconducting fluctuations boosted by a spatial distribution of critical temperatures in the sample. This interesting scenario should now be explored against the present precise determination of the transition lines, and the change of the specific heat anomaly.

Other open questions still remain. A first question concerns the large difference between the irreversibility line observed on the magnetostriction and the specific heat anomaly: it suggests a strong increase of the reversibility region in this phase, like the fact that the resistive transition only goes to zero when the bulk transition ends. This is similar to previous observations in UCoGe [69]. However an explanation for the suppression of the vortex pinning at high fields is still awaited.

Another important point concerns the order of the different transition lines and the precise slopes of the lines at the tricritical point. Indeed, as for $CeRh_2As_2$ [62], in the case of a spin-triplet to spin-singlet transition, a first-order transition is expected. In our specific heat measurements, we did not detect any hysteresis effects. The only features visible in Fig. 5 are a smaller jump of C/T for the LF to HF transition than along H_{c2} in the LF phase, as well as a slightly smaller width. This slight narrowing leaves open the possibility that the transition from LF to HF phases could be weakly first order. There are many cases in condensed matter physics where first-order transitions lead to negligible hysteresis: see, e.g., Ref. [70], or the old example of the ^{3}He melting curve. This point requires, however, further experimental investigations.

If this transition is first order, of course, the question of the tricritical point is solved. If it is not, it remains an issue to determine if there is an additional transition line within the LF superconducting phase, and whether or not the three transition lines determined in this work join with different slopes, or if the H_{c2} line has no change of slope (only a very strong positive curvature) at the tricritical point.

The entrance into the HF phase along H_{c2} cannot be done in a mixed singlet-triplet superconducting phase [71]: it would require, as for the chiral superconducting state [21], a double transition which is not observed.

Theoretical works based on microscopic calculations have predicted that the interplay between ferromagnetic and antiferromagnetic fluctuations [7,26] could lead to competing pairing interactions [26]. This competition could be central for both the pressure [26] and the field-induced phases of UTe_2. At ambient pressure, at the opposite of $CeRh_2As_2$, it could lead to a paradoxical spin-singlet phase at high fields, possibly driven by strong antiferromagnetic correlations on approaching the metamagnetic transition. Under pressure, this high-field phase would become the highest T_c phase with the lowering of the metamagnetic field along the b axis, whereas the pure spin-triplet phase would survive essentially for large enough fields along the easy a axis. UTe_2 is probably the first system where two competing pairing mechanisms of similar strength exist, and can be arbitrarily tuned by field or pressure: it is an ideal case to challenge theoretical models and understand which conditions allow for the emergence of spin-triplet superconductivity.

ACKNOWLEDGMENTS

We thank Y. Yanase, K. Miyake, M. Houzet, M. Zhitomirsky, and V. Mineev for very fruitful discussions, and A. Miyake and S. Imajo for kindly providing their data points. We received financial support from the CEA Exploratory program TOPOHALL, the French National Agency for Research ANR within the project FRESCO No. ANR-20-CE30-0020 and FETTOM No. ANR-19-CE30-0037, and from the JSPS programs KAKENHI (JP19H00646, JP20K20889, JP20H00130, JP20KK0061, JP20K03854, JP22H04933). We acknowledge support of the LNCMI-CNRS, member of the European Magnetic Field Laboratory (EMFL), and from the Laboratoire d'excellence LANEF (ANR-10-LABX-0051).

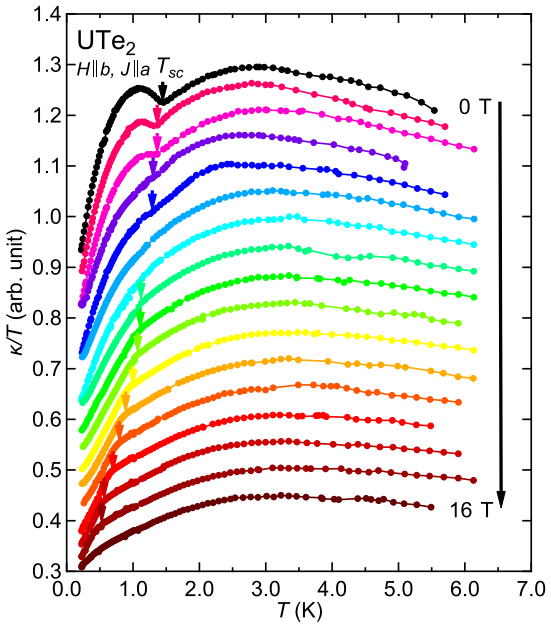

FIG. 17. Temperature dependence of κ/T in UTe_2 with $H\|b$ between 0 and 16 T (every Tesla). Traces have been shifted for clarity. The superconducting temperature T_c is represented by vertical arrows.

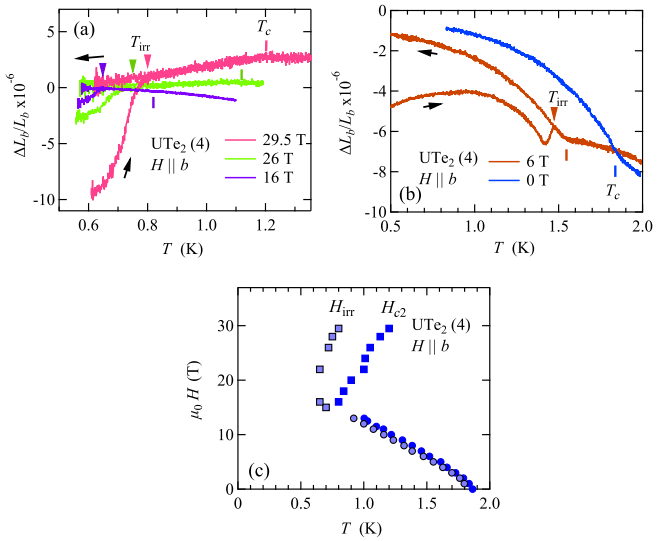

FIG. 18. Temperature dependence of the linear thermal expansion $\Delta L_b/L_b$ in UTe_2 with $H\|b$ at different magnetic fields measured in (a) the LNCMI Grenoble and (b) using a superconducting magnet. The arrows indicate the direction of the temperature sweep; see text for details. The temperature of the irreversibility field H_{irr} and the upper critical field H_{c2} are indicated by arrows and vertical bars, respectively. Panel (c) shows the phase diagram obtained from the thermal expansion measurements. While at low field ($H < 15$ T) $H_{irr} \approx H_{c2}$, at high fields the irreversibility line is much lower in temperature.

APPENDIX A: THERMAL CONDUCTIVITY $H \| b$

Thermal conductivity κ measurements have been performed on a sample from the same batch as sample 1. The temperature sweeps have been measured on a homemade dilution refrigerator with a base temperature of 100 mK and a superconducting magnet with field up to 16 T using a standard "one heater–two thermometers" setup. The temperature dependence of κ/T for different magnetic fields up to 16 T is represented in Fig. 17. κ/T shows a broad maximum at around 3 K. At low field, there is a clear increase in κ/T just below T_c, which is suppressed by increasing the field. Such an increase below T_c has also been observed in other systems such as $CeCoIn_5$ or YBCO and attributed to a suppression of the inelastic scattering of heat carriers (electrons and phonons, respectively) by the opening of the superconducting gap. In the case of UTe_2, the enhanced conductivity below T_c is likely due to an increase of the electronic mean free path due to the opening of the superconducting gap. At higher field ($\mu_0 H > 3$ T), entrance in the superconducting state is marked by a rapid decrease of the thermal conductivity, usually attributed to Andreev scattering on the vortex cores.

APPENDIX B: THERMAL EXPANSION FOR FIELD $H \| b$

As discussed in the main text, linear magnetostriction measurements are sensitive to pinning forces. Indeed, trapped flux imposes a field gradient at the sample surface, perpendicular to the applied field, controlled by the critical current density. Pinning force trapping magnetic flux lines on the lattice should be balanced by equal but opposite forces acting on the lattice. Hence, it can be shown that the length change of the crystal $\Delta L_b/L_b$ is proportional to $(H\Delta M/E)C_\nu$, where ΔM is the nonequilibrium part of the magnetization, E the Young modulus, and C_ν a constant depending on the Poisson ratio [53].

We also performed longitudinal thermal expansion measurements (length change in the field direction) on sample 4 as a function of temperature at fixed magnetic fields, which also show similar effects due to vortex pinning. The measurements were performed up to 29.5 T along the b axis in the high magnetic field laboratory LNCMI, and in addition using a superconducting magnet up to 13 T in the Pheliqs laboratory.

Figures 18(a) and 18(b) show the temperature dependence of the relative length change along the b axis $\Delta L_b/L_b$ for different magnetic fields. The data displayed in Fig. 18(a) are obtained by cooling from the normal state to the lowest temperature in a field 2 T below the target final field, then increasing the field at the lowest temperature up to the final field, heating at that field above T_c and cooling again. Increasing the field at low temperature induces a nonequilibrium magnetization inside the sample due to the flux pinning, while an equilibrium flux distribution occurs in the final field-cooled sweep. H_{irr} marks the onset of the irreversible magnetization regime.

The data in Fig. 18(b) are measured in a superconducting magnet using a dilution refrigerator. They are obtained from a similar procedure, however, starting by zero field cooling, then ramping the field up to its target value, heating up to the normal state and measuring the field-cooled length change. Again, the irreversibility line can be clearly determined.

In Fig. 18(c) we show the temperature dependence of the upper critical field H_{c2} and of the irreversibility field $H_{\rm irr}$ determined from the cycles described above. Data for $H \leq 13$ T are from the experiments performed in a superconducting magnet, while for $H > 13$ T they stem from the high-field experiments in LNCMI. While in the LF superconducting phase $H_{\rm irr}$ is lower but very close to H_{c2}, in the HF superconducting phase $H_{\rm irr}$ is far lower in temperature than H_{c2}, indicating a wide reversible region (with low pinning) behind H_{c2} in this state.

APPENDIX C: SPECIFIC HEAT: NORMAL PHASE

In general, the leading term of the specific heat of a heavy-fermion system at low temperatures ($T \ll T_F$, with T_F being the effective Fermi temperature), far from any quantum criticality, is linear in temperature: $C \propto \gamma T$.

The Sommerfeld coefficient γ is proportional to the density of states at the Fermi level, which is strongly renormalized compared to the free electron gas. In UTe_2, at low temperature, the competition between different natures of magnetic fluctuations (ferromagnetic or antiferromagnetic) as well as the role of valence fluctuations due to the interplay between U^{3+} and U^{4+} configurations may occur. The situation is even more complex in this system, because electronic correlations play the unusual role of driving the system from an insulating toward a metallic state [7,8,10,72].

As a consequence, even close to T_c, C/T is not the sum $\gamma + \beta T^2$ with βT^2 the phonon contribution far below the Debye temperature. An additional contribution is observed, likely coupled to the "Schottky-like" anomaly detected at $T^\star \approx 12$ K [58]. Figures 19(a) and 19(b) show C/T versus T^2 for sample 1 and sample 2. The phonon contribution has been calculated following the Debye model with a Debye temperature of $\theta_D = 180$ K [58]. Clearly, the phonon contribution is low compared to the measured specific heat and cannot reproduce the strong temperature increase of C/T at zero magnetic field. Under magnetic field, the anomaly at $T^\star$ shifts to higher temperatures for $H \| a$ and lower temperatures for $H \| b$. Accordingly, C/T strongly depends on the magnitude of the applied field and on its direction. Hence the low-temperature Sommerfeld coefficient γ cannot be determined properly from a direct analysis of the temperature dependence of C/T. We tried, as was done previously [46,47], to follow the field evolution of C/T at the lowest possible temperature, so as to be as close as possible to the value of γ. At 15 T for $H \| a$, C/T decreases with temperature (down to 0.3 K), which is quite unusual [Fig. 19(c)]. Thermoelectric power measurements have revealed the presence of several Lifshitz transitions in this field direction [39]. In the main text, the inset of Fig. 12 shows that the field dependence of C/T at 1.8 K has a minimum followed by a maximum close to 5 and 9 T, respectively. Moreover, field sweeps have been performed up to 31 T for $H \| a$, on a sample with a T_c of 1.45 K coming from the same batch as sample 1. Measurements of C/T are displayed in Fig. 20(a). A minimum (around 6 T) followed by a maximum (around 8 T) are visible for fields above the superconducting transition. At higher fields, a change of slope occurs for fields between 17 and 22 T, depending on the temperature,

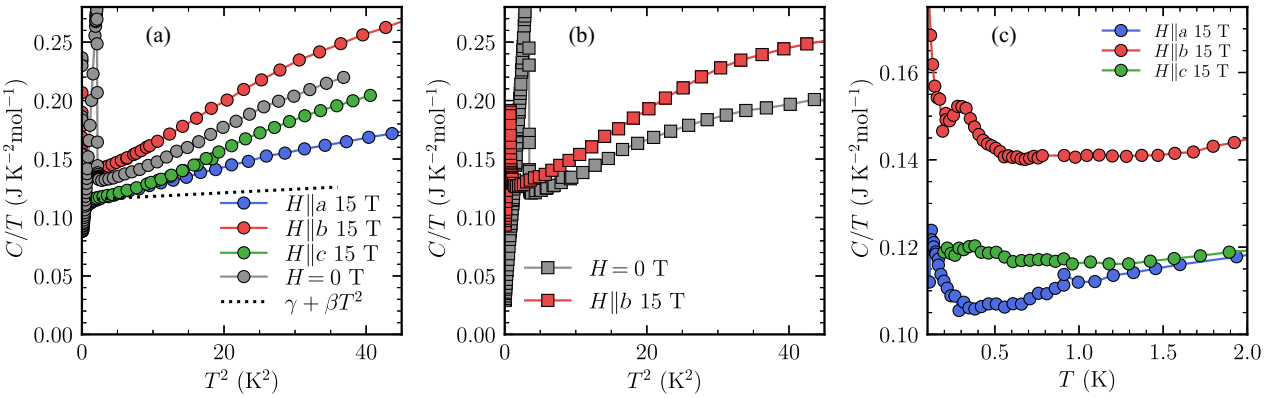

FIG. 19. Temperature dependence of C/T (sample 1) for fields applied along the three crystallographic directions. (a) C/T as a function of T^2, measured on sample 1: no linear behavior is seen. At 15 T for $H \| a$, the temperature dependence is drastically suppressed compared to measurements at 0 T, whereas it is slightly larger for $H \| b$. The dotted line is the sum of a constant Sommerfeld term and a phonon contribution estimated from a Debye temperature deduced from high-temperature measurements [58]. (b) Same data for $H \| b$ on sample 2: the anomalous magnetic contribution seems more pronounced than for sample 1. (c) C/T at low temperatures at 15 T along the three axes measured on sample 1. The superconducting transition at ~0.5 K remains visible for $H \| b$.

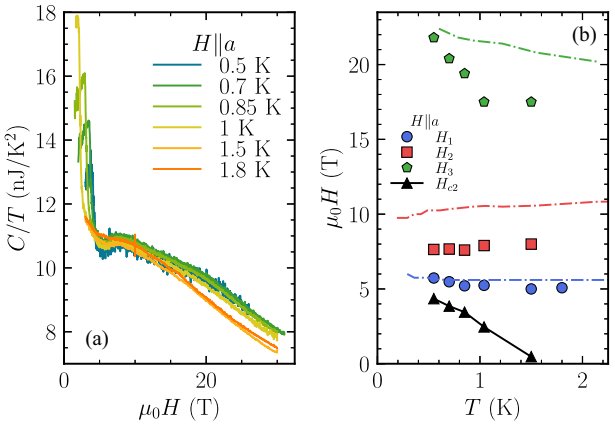

FIG. 20. (a) C/T measured for field sweeps at different temperatures with $H\|a$. Measurements done on a sample coming from the same batch as sample 1, with a T_c of 1.5 K. (b) Phase diagram $H\|a$ up to 31 T. Black triangles represent the superconducting transitions, blue circles are the minima of $C/T(H)$. Red squares represent the maxima of $C/T(H)$. Green pentagons represent the inflection point of C/T observed on field sweeps. The dash-dotted lines are the corresponding transitions measured by thermoelectric power in Ref. [39].

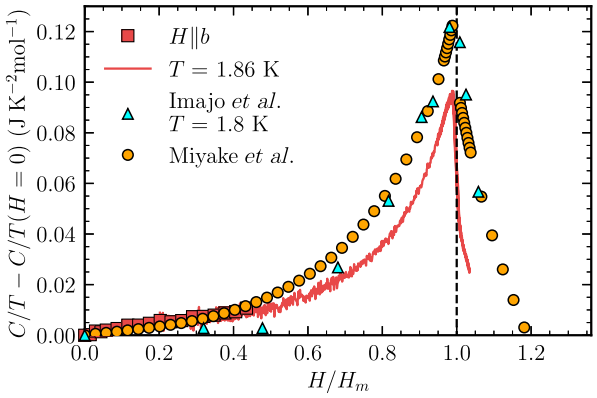

FIG. 21. Cyan triangles: specific heat measurements done in pulsed fields in Ref. [47]. Orange circles: $\gamma(H) - \gamma(H = 0)$ determined from the magnetization measurements through thermodynamic relations in Ref. [48]. Red line: our measurements.

where the magnetization along the a axis starts to saturate [46]. We can follow these three anomalies in addition to the superconducting transition, and establish the phase diagram shown in Fig. 20(b). The temperature dependence and the order of magnitude of the field where they occur are similar to those obtained from thermoelectric power measurements. The lower transition (at around 5–6 T) was clearly identified as a Lifshitz transition; the origin of the two others is less clear [39]. Regarding the present specific heat data, the origin of the pronounced maxima of C/T observed at ∼1 T for $H\|a$ and ∼1.5 T for $H\|c$ (Fig. 12 inset in the main text) is also not identified.

APPENDIX D: SPECIFIC HEAT: METAMAGNETIC TRANSITION

As regards the metamagnetic transition, we could measure precisely the field dependence of the anomaly, and check that it did not depend on field sweep rate, varied between ±350 and ±50 G/ sec. At this sweep rate, we also did not detect any magnetocaloric effect. Hence, the present continuous field sweep measurements show unambiguously that there is a jump at H_m, slightly broadened by a distribution of H_m. At 0.7 K, this jump of C/T leads to a decrease by 55 mJ K^{-2} mol^{-1} and the width of the transition is 0.25 T. This distribution of H_m possibly comes from the strong sensitivity of H_m to pressure [11,50] and most likely to stress (crystal defects could then generate this H_m distribution). Figure 21 shows the comparison of $C/T - C/T(H = 0)$ near $T = 1.8$ K for field along the b axis determined from our experiment performed on sample 3 and experiments performed in pulsed field. Reference [47] reports specific heat experiments in highly stabilized fields, using the long pulsed fields facility at ISSP. In Ref. [48] the Sommerfeld coefficient γ has been determined from the magnetization measurements $M(T)$ under pulsed fields, using Maxwell's relation for $H \neq H_m$ as $(\partial\gamma/\partial H)_T = (\partial^2 M/\partial T^2)_H$, and using the Clausius-Clapeyron relation for the first-order transition: $\mu_0 dH_m/dT = -\Delta S/\Delta M$ [48] to get the jump $\Delta\gamma = \Delta S/T$ at H_m. The last analysis indicated a discontinuous jump of $\Delta\gamma = -30$ mJ K^{-2} mol^{-1} at H_M for $H\|b$, which is lower than that obtained in the present experiment. However, despite some quantitative differences [e.g., the absolute variation of $C/T - C/T(H = 0)$ is larger in both pulsed field experiments] the general behavior is similar: an increase with H when approaching H_m and a drop at H_m followed by a strong decrease. A similar field dependence has been observed for the A coefficient of the electrical resistivity, albeit without a clear jump above H_m [15,45].

To extract the position and the width of the specific heat at the metamagnetic transition, it has been fitted like a broadened second-order phase transition, with the same Gaussian model as the superconducting transition. Fields replace temperatures, and H_m replaces T_c. H_m for the up sweeps are roughly constant at 34.75 T, and for the down sweeps H_m increases with the temperature. This goes along with the trend toward a closing of the hysteresis cycles with increasing temperatures, in agreement with the observations from resistivity measurements [45,59]. The width of the transitions increases abruptly from 0.24 to 0.45 T between 0.7 and 0.97 K and then stays constant with temperature. The jump of C/T at H_m strongly decreases on cooling from 0.97 to 0.7 K, otherwise, above 0.97 K, it decreases on warming. This anomaly at 0.7 K might be due to the presence of the HF transition, which is wide enough in field and temperature to influence the drop of C/T at H_m.

The nature of the magnetic correlations associated with the metamagnetic transition at H_m is an important issue, key to

identify the pairing mechanism responsible of the HF superconducting phase. The question is presently open. Indeed, Inelastic neutron experiments at such large fields are still not available. If the metamagnetic transition would occur along the easy axis like in UCoAl [73], the fluctuations would most likely be ferromagnetic, but it appears in UTe_2 along the hard axis. Other criteria like the value of the Wilson ratio, claimed to support ferromagnetic fluctuations at low fields due to its large value [58], would be of no help close to H_m: calculating this ratio on approaching H_m from raw data is certainly questionable in such a complex multiband system with local moment contributions. Moreover, this calculation would yield much smaller values than along the a axis at low fields: the susceptibility $\partial M/\partial H$ is at least 6 times smaller for $H\|b$ than for $H\|a$, and the specific heat increases almost by a factor 2 between zero field and H_m, suppressing the Wilson ratio deduced for $H\|a$ by at least a factor 10. Arguments for antiferromagnetic fluctuations exist, but are far from rock solid: besides the results from inelastic neutron measurements at low fields, we can note that the scaling relation found in many antiferromagnetic systems between the temperature of the maximum of the susceptibility $T_{\chi\,\max}$ (35 K) and the value of H_m [74] (33–35 T) is well obeyed in UTe_2.

APPENDIX E: SPECIFIC HEAT: SUPERCONDUCTING PHASE

1. Measurements in zero field

All measurements of C/T in UTe_2 display an upturn below 0.1 K and an extrapolated (from temperatures above the upturn) residual term at $T = 0$ which was quite large in the first measurements [4,6,43]. More recent studies are claiming that the residual term and the upturn are extrinsic to UTe_2 [13,44]. Our measurements on different samples in Fig. 22(a) show diverse behaviors at low temperatures. The upturn is not monotonously correlated to T_c; however, it is strongly reduced on our best samples. The residual term seems to be more systematically decreasing with the T_c increase, well in the trend reported in Ref. [13]. In any case, these measurements do agree with an extrinsic nature of these anomalies. Note also that on sample 2, the entropy balance is perfectly satisfied at T_c, within experimental errors (better than 1%). The low-temperature upturn plays a negligible role [see Fig. 22(b)].

2. Gaussian model for the specific heat anomaly

A simple hypothesis is that broadening of the specific heat transition is controlled by a Gaussian T_c distribution of the form:

$$p(T_c) = \frac{1}{\sigma\sqrt{2\pi}}\exp\left[-\frac{1}{2}\left(\frac{T_c - T_{c0}}{\sigma}\right)^2\right]. \tag{E1}$$

For the specific heat, or any additive quantity, we can then write that

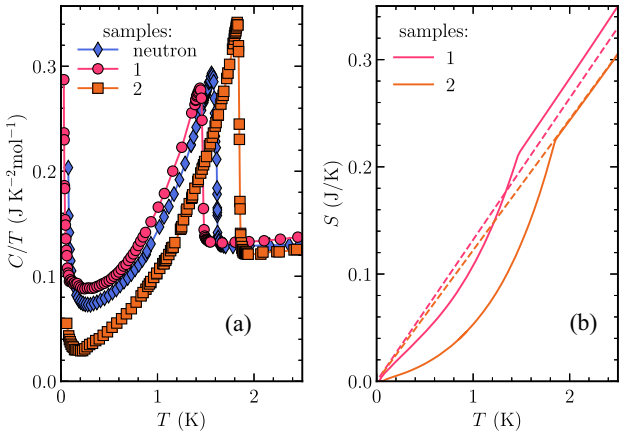

FIG. 22. (a) C/T as a function of temperature at zero field and low temperatures for different samples. Samples 1 and 2 are presented in this article. Sample neutron is a large sample of 241 mg used to perform the neutron diffusion experiments in Refs. [15,30]. (b) Entropy calculated for samples 1 and 2, showing the bad balance for 1 and the very good one for 2.

$$C/T = \int_{-\infty}^{\infty} p(T_c)C/T(T, T_c)dT_c. \tag{E2}$$

The simplest expression for $C/T(T, T_c)$ is a constant γ term above T_c, a jump at T_c followed by a constant positive slope below T_c. If both the slope and the jump are independent of T_c, this amounts to

$$C/T(T, T_c) = \gamma + \theta(T_c - T)\left(\frac{\Delta C}{T} + \alpha(T - T_c)\right). \tag{E3}$$

Hence, for the total specific heat:

$$\frac{C}{T}(T) = \gamma + \left(\frac{\Delta C}{T} + \alpha(T - T_{c0})\right)\left[\frac{1}{2} - \frac{1}{2}\mathrm{erf}\left(\frac{T - T_{c0}}{\sigma}\right)\right] - \alpha\frac{\sigma}{\sqrt{2\pi}}\exp\left[-\frac{1}{2}\left(\frac{T - T_{c0}}{\sigma}\right)^2\right]. \tag{E4}$$

This model is fine for the zero field transition, where $\Delta C/T$ is independent of T_c. However, under magnetic field, the broadening of the transition may correspond to a distribution of slopes of H_{c2} (proportional to T_c for clean type II superconductors). We can expect that $\Delta C/T$ will be suppressed with field, with a decrease controlled by $H/H_{c2}(0)$. Hence, $\Delta C/T$ will not be constant within the broadened transition. More simply, we can assume that the jump will be suppressed like $T_c(H)/T_c(0)$. The problem is therefore to relate $T_c(H)$ and $T_c(0)$, or more precisely, to get the $T_c(0)$ corresponding to a given $T_c(H)$. Then we could take for a model of the transition that $\Delta C/T$ is proportional, within the transition, to $T_c(H)/T_c(0)$. A simple way to find this relation is to assume a proportionality to the broadening so that

$$T_c(H) - T_{c0}(H) = \frac{\sigma}{\sigma_0}[T_c(0) - T_{c0}(0)],$$
$$\frac{\Delta C}{T}(T_c) = \frac{\Delta C}{T}(T_{c0})\frac{T_c/T_{c0}}{1 + \frac{\sigma_0}{\sigma}\frac{T_c - T_{c0}}{T_{c0}(0)}}. \quad \text{(E5)}$$

In the last expression, we wrote $T_c = T_c(H)$ and $T_{c0} = T_{c0}(H)$. As regards the slope, similarly, it should also depend on T_c. Indeed, in high fields, for example, where the temperature dependence of C/T is close to linear, the slope should depend both on T_c and on $\Delta C/T$. One way to keep some consistency within the transition is to assume that we have the same entropy balance for all the curves at different T_c at a given field. At low field, where $C/T(T)$ has no specific reason to remain close to linear far below T_c, there is no peculiar constraint on this entropy balance (the linear behavior of C/T below T_c is valid only close enough to T_c). However, for fields closer to $H_{c2}(0)$, we can expect that this entropy balance should be more or less close to zero. Explicitly, we can enforce that

$$\Delta S(T_c) = \int_0^{T_c}\left[\frac{\Delta C}{T}(T_c) + \alpha(T_c)(T - T_c)\right]dT = \beta T_c,$$

with β independent of T_c:

$$\alpha(T_c) = \frac{2}{T_c}\left[\frac{\Delta C}{T}(T_c) - \beta\right]. \quad \text{(E6)}$$

Inserting Eqs. (E5) and (E6) in Eqs. (E3) and (E2), we obtain a final expression for $C/T(T)$, easily managed in its integral form by numerical calculations. It depends linearly on the parameters γ, $(\Delta C/T)(T_{c0})$, and β (close to zero in high fields), and nonlinearly on σ and on T_{c0}. It has two additional inputs, taken from the zero field data: σ_0 and $T_{c0}(0)$.

APPENDIX F: MEASUREMENTS OF H_{c2} FOR $H \| a$

Three different samples have been measured and their H_{c2} determined from the specific heat anomaly for $H \| a$ including at very low fields. The results are shown in Fig. 23. The three samples come from different batches. Samples 1 and 2 have been measured with the same setup, and sample 5 with a different one. They all exhibit a strong negative curvature near T_c, proving that this feature is reproducible and intrinsic.

To our knowledge, there are at least two other cases among heavy-fermion superconductors showing also an anomalous behavior of H_{c2} at very low fields. The oldest one is UBe_{13} [75], however with a curvature which could be explained, for example, by a partial paramagnetic limitation [76]. The other is the ferromagnetic superconductor URhGe, which even has a vertical H_{c2} along the easy axis, up to the field (of order 50 mT) where a single domain is induced in the sample [77]. Such a mechanism is absent in UTe_2 which is paramagnetic and not ferromagnetic.

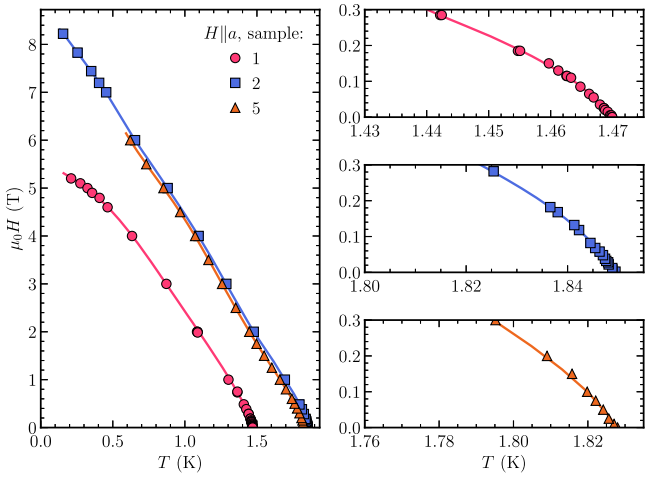

FIG. 23. H_{c2} of three different samples for $H \| a$: the anomalous strong curvature near T_c is reproducible, even for crystals with very different T_c.

APPENDIX G: MEASUREMENTS OF H_{c2} FOR $H \| b$: COMPARISON WITH RESISTIVITY

Resistivity has also been measured on the sample from which we cut off sample 3. The critical field obtained with $R = 0$ as criterion is compared to H_{c2} determined by specific heat. For the LF phase, as expected, $R = 0$ is above the specific heat transition. At low fields, there is a large difference between the initial slopes at T_c for the determination from resistivity or specific heat anomaly, most likely due to the sensitivity of resistivity

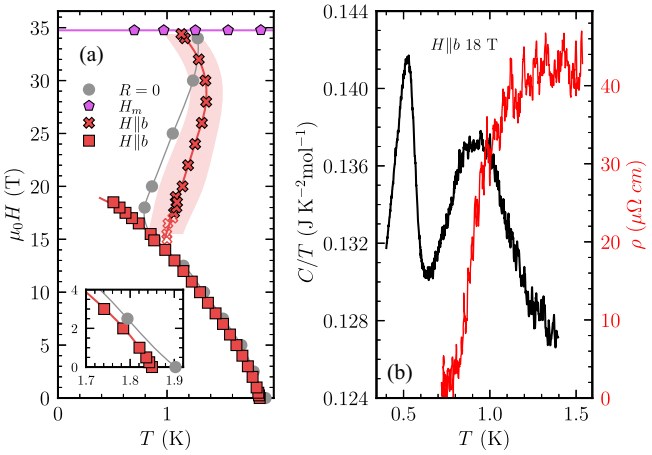

FIG. 24. (a) H_{c2} for $H \| b$ determined by C/T measurements (see main article). Gray points correspond to the $R = 0$ determined by resistivity measurements. The shaded region indicates the width of the HF transition. The inset is an enlargement for field below 4 T. (b) C/T as function of temperature compared to R as function of temperature, both measured at 18 T.

TABLE I. Values of the slope dH_{c1}/dT_c of H_{c1} at T_c from Ref. [54], the corresponding value of the calculated Ginzburg-Landau parameter κ, and the predicted value for dH_{c2}/dT_c for the sample of Ref. [54] (same batch as 1). For sample 2, dH_{c2}/dT_c is rescaled by the ratio of the T_c of these samples. The last column is the initial slope measured on sample 2.

	$-\frac{H_{c1}}{dT_c}$ (T/K) Ref. [54]	κ	$-\frac{H_{c2}}{dT_c}$ (T/K) Ref. [54]	$-\frac{H_{c2}}{dT_c}$ (T/K) Rescaled	$-\frac{H_{c2}}{dT_c}$ (T/K) Sample 2 measured
$H\|\|a$	0.001 13	202.683	16.052	20.480	20
$H\|\|b$	0.002 27	86.482	6.849	8.738	34.5
$H\|\|c$	0.002 52	75.838	6.006	7.663	7.5

measurements to filamentary superconductivity, rapidly suppressed by (small) magnetic fields. For the HF phase, $R = 0$ is below the maximum of the specific heat transition, which is more unusual. This can be seen in Fig. 24(b), showing the temperature dependence of C/T and of the resistivity at a fixed field of 18 T.

This discrepancy can arise from extrinsic inhomogeneities, like a continuous gradient of H_m in the sample, or from more intrinsic phenomena like a weaker pinning of vortices in the HF phase, which would induce a smaller critical current and possibly a shift of the resistive transition to lower temperatures. This is well known in organic superconductors [78] or in high-T_c cuprates [79], where the resistivity remains nonzero in the vortex liquid state, favored by the highly 2D anisotropy of their normal and superconducting properties. It has also been observed in iron-based superconductors [80], and like in the organics or high-T_c cuprates, with much stronger differences on the T_c determination than observed in UTe_2. The difficulty for such an explanation in UTe_2 is the same as faced for UCoGe [69]: the systems are 3D rather than 2D; hence, superconducting fluctuations should be much less effective. In addition, the discrepancy between resistivity and specific heat determination of H_{c2} occurs only at very high fields, whereas in the other systems, it arises very fast when entering the mixed state. It could be that the quantitative difference in the effect arises precisely because superconducting fluctuations are much less important in UTe_2 or UCoGe than in the quasi-2D systems. However, it remains to be explained why this would happen only in the field-reinforced phase. This point remains a fully open question.

APPENDIX H: COMPARISON OF H_{c2} AND H_{c1}

In the Ginzburg-Landau regime near T_c, well-known relations exist between the lower, upper, and thermodynamic critical fields. They are expressed through an anisotropic Ginzburg-Landau parameter κ:

$$H_{c1} = \frac{H_c}{\sqrt{2}\kappa}[\ln(\kappa) + 0.49],$$
$$H_{c2} = \sqrt{2}\kappa H_c. \tag{H1}$$

The thermodynamic critical field $H_c(T)$ is determined by double integration of the specific heat at 0 T, and we obtain a slope at T_c of $(dH_c/dT_c) = -0.057$ T/K for the sample of Ref. [54] ($(dH_c/dT_c) = -0.0685$ T/K for sample 2). H_{c1} has been measured on a crystal of the same batch as 1 in all field directions [54]. We can determine κ in the three directions from the first equation (H1), and extract from the second a prediction for the value of dH_{c2}/dT_c of sample 1 as well as of sample 2 by rescaling dH_{c2}/dT_c with the ratio of their respective T_c. These values are reported in Table I. The large value of dH_{c2}/dT_c at T_c for $H\|a$ is in very good agreement with the values of dH_{c1}/dT_c as predicted by the Ginzburg-Landau relations. This is also true for $H\|c$, but not for $H\|b$.

Figure 25(a) shows H_{c2} determined by specific heat on sample 2 and dH_{c2}/dT_c at T_c calculated from H_{c1}. The inset of Fig. 25(a) shows how the predicted dH_{c2}/dT_c matches the present measurement for $H\|a$ very close to T_c. The strong disagreement for $H\|b$ as well as the difference between the slope of H_{c2} at T_c and the linear regime at lower temperatures for $H\|a$ are clearly visible in the main

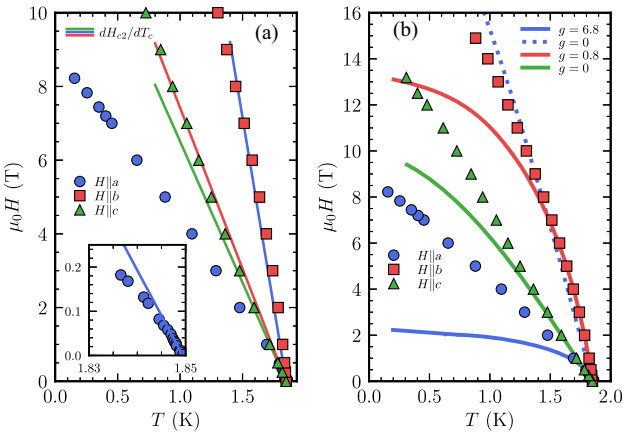

FIG. 25. (a) H_{c2} measurements on sample 2: lines show dH_{c2}/dT_c calculated and rescaled from dH_{c1}/dT_c determined in Ref. [54]. The inset is an enlargement for fields $H\|a$ below 0.25 T. There is a very good agreement between H_{c1} and H_{c2} for $H\|a$ and $H\|c$, but a strong discrepancy for $H\|b$. (b) H_{c2} determined by specific heat on sample 2. The lines are the best adjustment of H_{c2} (orbital and paramagnetic limitations) to match the measured initial slopes and curvatures in each direction. The dotted line corresponds to a pure orbital limitation of H_{c2} adjusted on its initial slope for $H\|a$, evidencing the very strong negative curvature close to T_c. g is the gyromagnetic factor and λ is set to 1.

panel of Fig. 25(a). By contrast, the linear regime for $H\|c$ does match the Ginzburg-Landau prediction in a large temperature range.

APPENDIX I: STRONG-COUPLING MODEL FOR H_{c2}

The model used for the calculation of H_{c2} in the strong-coupling regime is fully described in Ref. [81]. It extends that of Ref. [82] to include the paramagnetic limitation mechanism. For completeness, we present here the basic equations. This model is derived from the Eliashberg theory for electron-phonon interaction in s-wave superconductors. We believe that it remains relevant for the estimation of strong-coupling effects on the upper critical field in unconventional superconductors (anyhow, we do not know of such calculation for p-wave superconductors).

A most simplified form of the Eliashberg interaction is used, sufficient to capture the most important properties of the strong-coupling regime: the renormalization of the Fermi velocity and the pair-breaking effects arising from the presence of thermal phonons (or magnetic excitations) close to T_c when the strong-coupling constant λ gets large. The spectral density of interaction is taken as a simple δ function (Einstein spectrum):

$$\alpha^2 F(\omega) = \left(\frac{\lambda\Omega}{2}\right)\delta(\omega-\Omega), \tag{I1}$$

where ω is the frequency, Ω the characteristic energy of the interactions (of order the Debye temperature for electron-phonon interaction), and λ is the dimensionless strong-coupling constant. H_{c2} is then determined by a system of linear equations for the gap:

$$\Delta(i\tilde{\omega}_n) = \left(\frac{\pi T}{\Omega}\right)\sum_{|\omega_m|<\omega_c}[\lambda(\omega_n-\omega_m)-\mu^*]\chi(\tilde{\omega}_m)\Delta(i\tilde{\omega}_m), \tag{I2}$$

where $\omega_n = \pi T(2n+1)$ are Matsubara frequencies, μ^* is the screened Coulomb pseudo potential, ω_c is a frequency cutoff (8–10 times Ω), and

$$\tilde{\omega}_n = \omega_n + \pi T\sum_m \lambda(\omega_n-\omega_m)\mathrm{sgn}(\omega_n),$$
$$\lambda(\omega_n-\omega_m) = \frac{\lambda\Omega^2}{\Omega^2+(\omega_n-\omega_m)^2}. \tag{I3}$$

The function $\chi(\tilde{\omega}_n)$ in Eq. (I2) contains the effects of the field (B) on the gap equations through the orbital and paramagnetic effects:

$$\chi(\tilde{\omega}_n) = \int_0^\infty dx \frac{\beta\exp(-\beta x)}{\sqrt{\tilde{Q}^2+x}}\tan^{-1}\left(\frac{\sqrt{\tilde{Q}^2+x}}{\frac{|\tilde{\omega}_n|+ig\mu_B B/2\mathrm{sgn}(\tilde{\omega}_n)}{\Omega}}\right). \tag{I4}$$

Here $\beta = [2\Omega^2/\hbar eB(\bar{v}_F^{\mathrm{bare}})^2]$ parametrizes the orbital effect: $\bar{v}_F^{\mathrm{bare}}$ is a bare average Fermi velocity (meaning a Fermi velocity not renormalized by the pairing interaction), perpendicular to the applied magnetic field, and e is the elementary charge. The paramagnetic limit is parametrized by the gyromagnetic factor g in the direction of the applied field. Moreover, $\tilde{Q} = (\hbar\bar{v}_F^{\mathrm{bare}}Q/2\Omega)$ is the dimensionless amplitude of the (potential) Fulde-Ferrel, Larkin-Ovchinnikov (FFLO) wave vector, which has to be taken into account for dominant paramagnetic limit. Hence for nonvanishing g, the system of Eq. (I2) has to be solved (with the usual techniques of linear algebra) optimizing the solution with respect to Q for maximum H_{c2}: for dominant paramagnetic limitation, a finite Q marking the entrance in the FFLO state can be found for temperatures below $0.55T_c$.

APPENDIX J: FIELD DEPENDENCE OF THE PAIRING STRENGTH MODELED BY A STRONG-COUPLING PARAMETER λ

Figure 25(b) shows H_{c2} along the three crystallographic directions, calculated with the strong-coupling model for the upper critical field already used in Refs. [11,37] and summarized in Appendix I, at fixed pairing strength. The measured initial slopes dH_{c2}/dT_c at T_c are controlled by the orbital limit, hence by v_F. The strong-coupling constant λ is set to 1, which seems a reasonable value for UTe_2. The plain lines in Fig. 25(b) are $H_{c2}(T)$ calculated with the orbital limit adjusted to match the measured dH_{c2}/dT_c, and the gyromagnetic factor g adjusted to match the initial negative curvature along the a and b axes ($g=6.5$ along the a axis and $g=0.8$ along the b axis). Deviations of the measured H_{c2} to such a usual combined orbital and paramagnetic limitation are observed for all applied directions of the magnetic field.

To explain these deviations, a field-dependent pairing strength is assumed. It is extracted from the data through a calculation of $H_{c2}(T)$ at fixed values of λ (see Fig. 13 of the main text for the case of $H\|b$). The typical energy controlling T_c (Ω), the Coulomb repulsion parameter μ^*, and the bare average Fermi velocity for field along the i axis ($\bar{v}_{F0}^{\mathrm{bare},i}$) controlling the orbital limit are taken independent of λ. The effective Fermi velocity controlling the orbital limit and so dH_{c2}/dT_c (at fixed λ) is renormalized as $\bar{v}_F^i = (\bar{v}_{F0}^{\mathrm{bare},i}/1+\lambda)$. If λ is field dependent, this effective Fermi velocity is also field dependent. In Table II, we also calculate the Fermi velocity along each i axis: v_F^i, deduced from the effective Fermi velocities through $v_F^i = (\bar{v}_F^j\bar{v}_F^k/\bar{v}_F^i)$, where j, k are the axis perpendicular to i.

It is to be noted that the lowest Fermi velocities (v_F) are along the b and c axes and highest along a axis.

TABLE II. Parameter values of the fit. We used a strong-coupling parameter $\lambda(H=0)=1$, with a typical energy (equivalent to the Debye energy) $\Omega = 28.4$ K, $\mu^* = 0.1$, pair-breaking impurity scattering rate $\Gamma = 1.39$ K. Values of $\bar{v}_F$ used in the fit are reported for each field direction. Difference between $\bar{v}_F^i$ and v_F^i is explained in the text. The corresponding coherence lengths are calculated from and $\xi_0 = 0.18(\hbar v_F/k_B T_c)$.

	$\bar{v}_F^i(H=0)$ (m/sec)	g	$\bar{\xi}_0^i$ (Å)	$v_F^i(H=0)$ along i axis	ξ_0^i (Å) along i axis
$H\|\|a$	5400	0	40	14 400	106
$H\|\|b$ (LF)	8600	0	64	5680	42
$H\|\|c$	9044	0	67	5130	38
$H\|\|b$ (HF)	8600	2	64	5680	42

This matches qualitatively the anisotropy found in transport measurements between the different axes [83]. Quantitatively, H_{c2} depends on an average of the Fermi velocities perpendicular to the applied field direction, weighted by the pairing strength. As a consequence, for example, we never succeeded to compare quantitatively anisotropies of H_{c2} in UPt_3 or in URu_2Si_2 with the detailed determination of their respective Fermi surfaces by quantum oscillations [84,85], even though the order of magnitude of the orbital limitation is consistent with measured effective Fermi velocities. This is probably even more acute if subtle $\boldsymbol{Q}$-dependent pairing is responsible for the specific pairing state realized in the system, as could well be the case in UTe_2 [7,26,34,35].

For $H\|a$, as discussed in the main text, we have chosen the most natural hypothesis of an ESP (equal-spin-pairing) state along the a axis, hence no paramagnetic limitation of H_{c2}, an initial slope matching the measured one (agreement with H_{c1}) implying a suppression of the pairing strength under field. However, it is also possible to construct a model where the pairing strength would increase along the a axis. Indeed, maintaining an initial slope matching the measured one, if we suppose that the g factor is in reality ≥ 6.8, the same fitting procedure will lead to a field increase of $\lambda(H)$.

We rejected this scenario due to the very large and rather unrealistic value required for the g factor and the strong contradiction with NMR Knight-shift measurements observing no change at all for $H\|a$ [14]. It should be stressed here that NMR measurements are performed at fixed field. They yield the change of electronic spin susceptibility across T_c from the temperature variation of the Knight shift. Hence, this measurement is not directly influenced by the field dependence of the pairing strength, as opposed to considerations on the violation of the paramagnetic limit on H_{c2}.

APPENDIX K: BROADENING OF THE SPECIFIC HEAT TRANSITION BY A DISTRIBUTION OF H_m

As explained in Appendix D, we could extract a standard deviation $\sigma = 0.19$ T for the distribution of H_m, hence a relative standard deviation $(\sigma/H_m) \sim 0.55\%$

As explained in the main text (Fig. 13), from the calculation of H_{c2} at fixed values of the pairing strength λ, we can extract also the superconducting critical temperature under field as

$$T_c = \varphi\left[H, \tilde{\lambda}\left(\frac{H}{H_m}\right)\right],$$
$$\tilde{\lambda}\left(\frac{H}{H_m}\right) = \lambda\left(H\frac{H_{m0}}{H_m}\right), \tag{K1}$$

where H_{m0} is the center of the distribution of metamagnetic fields H_m, determined from the specific heat measurements of the metamagnetic transition. $\lambda(H)$ is the field-dependent pairing strength deduced from the different models for H_{c2} and drawn in Fig. 14 of the main text.

From this relation, we can calculate the effect of a Gaussian distribution of H_m on the specific heat anomaly at constant field of the superconducting transition, using for C/T [instead of Eq. (E2)]:

$$C/T = \int p(H_m) C/T[T, T_c(H, H_m)] dH_m. \tag{K2}$$

This is the way we could draw the broadening of the specific heat anomaly in Figs. 15 and 16 of the main text, using the two different determinations of $\lambda(H/H_m)$ (with or without paramagnetic limitation of H_{c2}).

However, even without a full determination of the shape of the anomaly, requiring a numerical integration of Eq. (K2), we can understand why the broadening is larger when there is a paramagnetic limitation of H_{c2}. From Eq. (K1), we can derive the derivative of T_c with respect to H_m at fixed H and for $H_m = H_{m0}$. It measures the sensitivity of T_c to H_m, hence the broadening of the C/T anomaly due to a distribution of H_m:

$$\left.\frac{\partial T_c}{\partial H_m}\right|_H = \left.\frac{\partial T_c}{\partial \lambda}\right|_H \left(-\frac{H}{H_{m0}}\right)\left(\frac{d\lambda}{dH}\right). \tag{K3}$$

When comparing both models, it is clear that one has a stronger field dependence of λ than the other, but this could be compensated by a different $(\partial T_c/\partial\lambda)|_H$ which has to be computed at finite field [on the $H_{c2}(T)$ line]. Indeed, both

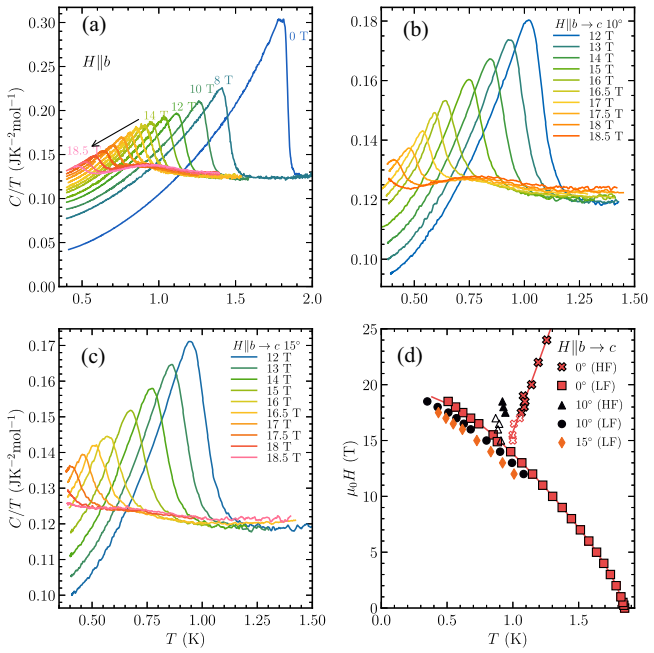

FIG. 26. C/T as a function of temperature for several fields between 0 and 18.5 T, measured on sample 3. (a) C/T for $H\|b$, (b) for an angle of 10° toward the c axis, (c) for an angle of 15° toward the c axis, and (d) evolution of the upper critical field H_{c2} and of the transition between the LF and HF phases with angle in the (b,c) plane, from analysis of the data in panels (a–c).

models share the same $H_{c2}(T)$. We can compute its temperature derivative (at $H_m = H_{m0}$) from Eq. (K1):

$$dT = \left.\frac{\partial T_c}{\partial H}\right|_\lambda dH_{c2} + \left.\frac{\partial T_c}{\partial \lambda}\right|_H \left(\frac{H_{m0}}{H_m}\right)\left(\frac{d\lambda}{dH}\right) dH_{c2},$$

$$\frac{dT}{dH_{c2}} - \left.\frac{\partial T_c}{\partial H}\right|_\lambda = -\left(\frac{H_{m0}}{H}\right)\left.\frac{\partial T_c}{\partial H_m}\right|_H. \quad \text{(K4)}$$

The last equation shows that the difference between models for $(\partial T_c/\partial H_m)|_H$ arises not directly from $(d\lambda/dH)$, but rather from $(\partial T_c/\partial H)|_\lambda$: so the flatter $H_{c2}(T)$ at fixed λ, the stronger the broadening. Hence a paramagnetic limitation of H_{c2} arising for singlet pairing will lead to much broader transitions than a H_{c2} controlled by a pure orbital limit, as is the case for a spin-triplet ESP state (see Fig. 13 in the main text).

APPENDIX L: ANGULAR DEPENDENCE OF THE SPECIFIC HEAT IN THE (b, c) PLANE

ac specific heat measurements have been performed on sample 2 up to 18.5 T for several angles in the (b, c) plane. Figures 26(a)–26(c) show temperature sweeps for different fields for angles of 0°, 10°, and 15° from b toward the c axis. As the field is rotated toward the c axis, the sharp transition of the LF phase is shifted toward lower temperatures. The same behavior is observed for the wide transition of the HF phase. The corresponding critical temperatures for the two transitions at the different angles are reported on the phase diagram of Fig. 26(d), using the same Gaussian analysis as in the main text. For H_{c2} at 15°, it was impossible to extract a reliable value of T_c for the HF transition.

[1] L. Fu and C. L. Kane, *Superconducting Proximity Effect and Majorana Fermions at the Surface of a Topological Insulator*, Phys. Rev. Lett. **100**, 096407 (2008).

[2] A. J. Leggett, *A Theoretical Description of the New Phases of Liquid* ^{3}He, Rev. Mod. Phys. **47**, 331 (1975).

[3] R. Joynt and L. Taillefer, *The Superconducting Phases of* UPt_3, Rev. Mod. Phys. **74**, 235 (2002).

[4] D. Aoki, K. Ishida, and J. Flouquet, *Review of U-Based Ferromagnetic Superconductors: Comparison between* UGe_2, URhGe, *and* UCoGe, J. Phys. Soc. Jpn. **88**, 022001 (2019).

[5] S. K. Ghosh, M. Smidman, T. Shang, J. F. Annett, A. D. Hillier, J. Quintanilla, and H. Yuan, *Recent Progress on Superconductors with Time-Reversal Symmetry Breaking*, J. Phys. Condens. Matter **33**, 033001 (2020).

[6] S. Ran, C. Eckberg, Q.-P. Ding, Y. Furukawa, T. Metz, S. R. Saha, I.-L. Liu, M. Zic, H. Kim, J. Paglione, and N. P. Butch, *Nearly Ferromagnetic Spin-Triplet Superconductivity*, Science **365**, 684 (2019).

[7] Y. Xu, Y. Sheng, and Y.-f. Yang, *Quasi-Two-Dimensional Fermi Surfaces and Unitary Spin-Triplet Pairing in the Heavy Fermion Superconductor* UTe_2, Phys. Rev. Lett. **123**, 217002 (2019).

[8] J. Ishizuka, S. Sumita, A. Daido, and Y. Yanase, *Insulator-Metal Transition and Topological Superconductivity in* UTe_2 *from a First-Principles Calculation*, Phys. Rev. Lett. 2019) 217001 ,**123**).

[9] A. B. Shick, S.-i. Fujimori, and W. E. Pickett, UTe_2*: A Nearly Insulating Half-Filled* $j = \frac{5}{2}$ $5f^3$ *Heavy-Fermion Metal*, Phys. Rev. B **103**, 125136 (2021).

[10] D. Aoki, A. Nakamura, F. Honda, D. Li, Y. Homma, Y. Shimizu, Y. J. Sato, G. Knebel, J.-P. Brison, A. Pourret, D. Braithwaite, G. Lapertot, Q. Niu, M. Vališka, H. Harima, and J. Flouquet, *Unconventional Superconductivity in Heavy Fermion* UTe_2, J. Phys. Soc. Jpn. **88**, 043702 (2019).

[11] G. Knebel, W. Knafo, A. Pourret, Q. Niu, M. Vališka, D. Braithwaite, G. Lapertot, M. Nardone, A. Zitouni, S. Mishra, I. Sheikin, G. Seyfarth, J.-P. Brison, D. Aoki, and J. Flouquet, *Field-Reentrant Superconductivity Close to a Metamagnetic Transition in the Heavy-Fermion Superconductor* UTe_2, J. Phys. Soc. Jpn. **88**, 063707 (2019).

[12] S. Ran, I.-L. Liu, Y. S. Eo, D. J. Campbell, P. M. Neves, W. T. Fuhrman, S. R. Saha, C. Eckberg, H. Kim, D. Graf, F. Balakirev, J. Singleton, J. Paglione, and N. P. Butch, *Extreme Magnetic Field-Boosted Superconductivity*, Nat. Phys. **15**, 1250 (2019).

[13] D. Aoki, J.-P. Brison, J. Flouquet, K. Ishida, G. Knebel, Y. Tokunaga, and Y. Yanase, *Unconventional Superconductivity in* UTe_2, J. Phys. Condens. Matter **34**, 243002 (2022).

[14] H. Fujibayashi, G. Nakamine, K. Kinjo, S. Kitagawa, K. Ishida, Y. Tokunaga, H. Sakai, S. Kambe, A. Nakamura, Y. Shimizu, Y. Homma, D. Li, F. Honda, and D. Aoki,

Superconducting Order Parameter in UTe_2 *Determined by Knight Shift Measurement*, J. Phys. Soc. Jpn. **91**, 043705 (2022).

[15] W. Knafo, G. Knebel, P. Steffens, K. Kaneko, A. Rosuel, J.-P. Brison, J. Flouquet, D. Aoki, G. Lapertot, and S. Raymond, *Low-Dimensional Antiferromagnetic Fluctuations in the Heavy-Fermion Paramagnetic Ladder Compound* UTe_2, Phys. Rev. B **104**, L100409 (2021).

[16] S. Ran, S. R. Saha, I.-L. Liu, D. Graf, J. Paglione, and N. P. Butch, *Expansion of the High Field-Boosted Superconductivity in* UTe_2 *under Pressure*, npj Quantum Mater. **6**, 75 (2021).

[17] D. Braithwaite, M. Vališka, G. Knebel, G. Lapertot, J. P. Brison, A. Pourret, M. E. Zhitomirsky, J. Flouquet, F. Honda, and D. Aoki, *Multiple Superconducting Phases in a Nearly Ferromagnetic System*, Commun. Phys. **2**, 147 (2019).

[18] W.-C. Lin, D. J. Campbell, S. Ran, I.-L. Liu, H. Kim, A. H. Nevidomskyy, D. Graf, N. P. Butch, and J. Paglione, *Tuning Magnetic Confinement of Spin-Triplet Superconductivity*, npj Quantum Mater. **5**, 68 (2020).

[19] D. Aoki, F. Honda, G. Knebel, D. Braithwaite, A. Nakamura, D. X. Li, Y. Homma, Y. Shimizu, Y. J. Sato, J. P. Brison, and J. Flouquet, *Multiple Superconducting Phases and Unusual Enhancement of the Upper Critical Field in* UTe_2, J. Phys. Soc. Jpn. **89**, 053705 (2020).

[20] S. M. Thomas, C. Stevens, F. B. Santos, S. S. Fender, E. D. Bauer, F. Ronning, J. D. Thompson, A. Huxley, and P. F. S. Rosa, *Spatially Inhomogeneous Superconductivity in* UTe_2, Phys. Rev. B **104**, 224501 (2021).

[21] I. M. Hayes, D. S. Wei, T. Metz, J. Zhang, Y. S. Eo, S. Ran, S. R. Saha, J. Collini, N. P. Butch, D. F. Agterberg, A. Kapitulnik, and J. Paglione, *Multicomponent Superconducting Order Parameter in* UTe_2, Science **373**, 797 (2021).

[22] L. Jiao, S. Howard, S. Ran, Z. Wang, J. O. Rodriguez, M. Sigrist, Z. Wang, N. P. Butch, and V. Madhavan, *Chiral Superconductivity in Heavy-Fermion Metal* UTe_2, Nature (London) **579**, 523 (2020).

[23] P. F. S. Rosa, A. Weiland, S. S. Fender, B. L. Scott, F. Ronning, J. D. Thompson, E. D. Bauer, and S. M. Thomas, *Single Thermodynamic Transition at 2 K in Superconducting* UTe_2 *Single Crystals*, Commun. Mater. **3**, 33 (2022).

[24] Y. Iguchi, H. Man, S. M. Thomas, F. Ronning, P. F. S. Rosa, and K. A. Moler, *Microscopic Imaging Homogeneous and Single Phase Superfluid Density in* UTe_2, arXiv:2210.09562.

[25] T. Shishidou, H. G. Suh, P. M. R. Brydon, M. Weinert, and D. F. Agterberg, *Topological Band and Superconductivity in* UTe_2, Phys. Rev. B **103**, 104504 (2021).

[26] J. Ishizuka and Y. Yanase, *Periodic Anderson Model for Magnetism and Superconductivity in* UTe_2, Phys. Rev. B **103**, 094504 (2021).

[27] C. Duan, K. Sasmal, M. B. Maple, A. Podlesnyak, J.-X. Zhu, Q. Si, and P. Dai, *Incommensurate Spin Fluctuations in the Spin-Triplet Superconductor Candidate* UTe_2, Phys. Rev. Lett. **125**, 237003 (2020).

[28] N. P. Butch, S. Ran, S. R. Saha, P. M. Neves, M. P. Zic, J. Paglione, S. Gladchenko, Q. Ye, and J. A. Rodriguez-Rivera, *Symmetry of Magnetic Correlations in Spin-Triplet Superconductor* UTe_2, npj Quantum Mater. **7**, 39 (2022).

[29] C. Duan, R. E. Baumbach, A. Podlesnyak, Y. Deng, C. Moir, A. J. Breindel, M. B. Maple, E. M. Nica, Q. Si, and P. Dai, *Resonance from Antiferromagnetic Spin Fluctuations for Superconductivity in* UTe_2, Nature (London) **600**, 636 (2021).

[30] S. Raymond, W. Knafo, G. Knebel, K. Kaneko, J.-P. Brison, J. Flouquet, D. Aoki, and G. Lapertot, *Feedback of Superconductivity on the Magnetic Excitation Spectrum of* UTe_2, J. Phys. Soc. Jpn. **90**, 113706 (2021).

[31] G. Aeppli, E. Bucher, C. Broholm, J. K. Kjems, J. Baumann, and J. Hufnagl, *Magnetic Order and Fluctuations in Superconducting* UPt_3, Phys. Rev. Lett. **60**, 615 (1988).

[32] T. Nomoto and H. Ikeda, *Exotic Multigap Structure in* UPt_3 *Unveiled by a First-Principles Analysis*, Phys. Rev. Lett. **117**, 217002 (2016).

[33] T. Hazra and P. Coleman, *Triplet Pairing Mechanisms from Hund's-Kondo Models: Applications to* UTe_2 *and* $CeRh_2As_2$, arXiv:2205.13529.

[34] L. Chen, H. Hu, C. Lane, E. M. Nica, J.-X. Zhu, and Q. Si, *Multiorbital Spin-Triplet Pairing and Spin Resonance in the Heavy-Fermion Superconductor* UTe_2, arXiv:2112.14750.

[35] A. Kreisel, Y. Quan, and P. J. Hirschfeld, *Spin-Triplet Superconductivity Driven by Finite-Momentum Spin Fluctuations*, Phys. Rev. B **105**, 104507 (2022).

[36] T. Hattori, Y. Ihara, Y. Nakai, K. Ishida, Y. Tada, S. Fujimoto, N. Kawakami, E. Osaki, K. Deguchi, N. K. Sato, and I. Satoh, *Superconductivity Induced by Longitudinal Ferromagnetic Fluctuations in UCoGe*, Phys. Rev. Lett. **108**, 066403 (2012).

[37] B. Wu, G. Bastien, M. Taupin, C. Paulsen, L. Howald, D. Aoki, and J.-P. Brison, *Pairing Mechanism in the Ferromagnetic Superconductor UCoGe*, Nat. Commun. **8**, 14480 (2017).

[38] V. P. Mineev, *Phase Diagram of UCoGe*, Phys. Rev. B **95**, 104501 (2017).

[39] Q. Niu, G. Knebel, D. Braithwaite, D. Aoki, G. Lapertot, G. Seyfarth, J.-P. Brison, J. Flouquet, and A. Pourret, *Fermi-Surface Instability in the Heavy-Fermion Superconductor* UTe_2, Phys. Rev. Lett. **124**, 086601 (2020).

[40] Q. Niu, G. Knebel, D. Braithwaite, D. Aoki, G. Lapertot, M. Vališka, G. Seyfarth, W. Knafo, T. Helm, J.-P. Brison, J. Flouquet, and A. Pourret, *Evidence of Fermi Surface Reconstruction at the Metamagnetic Transition of the Strongly Correlated Superconductor* UTe_2, Phys. Rev. Res. **2**, 033179 (2020).

[41] B. Michon, C. Girod, S. Badoux, J. Kačmarčík, Q. Ma, M. Dragomir, H. A. Dabkowska, B. D. Gaulin, J.-S. Zhou, S. Pyon, T. Takayama, H. Takagi, S. Verret, N. Doiron-Leyraud, C. Marcenat, L. Taillefer, and T. Klein, *Thermodynamic Signatures of Quantum Criticality in Cuprate Superconductors*, Nature (London) **567**, 218 (2019).

[42] R. Küchler, T. Bauer, M. Brando, and F. Steglich, *A Compact and Miniaturized High Resolution Capacitance Dilatometer for Measuring Thermal Expansion and Magnetostriction*, Rev. Sci. Instrum. **83**, 095102 (2012).

[43] T. Metz, S. Bae, S. Ran, I.-Lin Liu, Y. S. Eo, W. T. Fuhrman, D. F. Agterberg, S. M. Anlage, N. P. Butch, and J. Paglione, *Point-Node Gap Structure of the Spin-Triplet Superconductor* UTe_2, Phys. Rev. B **100**, 220504(R) (2019).

[44] L. P. Cairns, C. R. Stevens, C. D. O'Neill, and A. Huxley, *Composition Dependence of the Superconducting Properties of* UTe_2, J. Phys. Condens. Matter **32**, 415602 (2020).
[45] W. Knafo, M. Vališka, D. Braithwaite, G. Lapertot, G. Knebel, A. Pourret, J.-P. Brison, J. Flouquet, and D. Aoki, *Magnetic-Field-Induced Phenomena in the Paramagnetic Superconductor* UTe_2, J. Phys. Soc. Jpn. **88**, 063705 (2019).
[46] A. Miyake, Y. Shimizu, Y. J. Sato, D. Li, A. Nakamura, Y. Homma, F. Honda, J. Flouquet, M. Tokunaga, and D. Aoki, *Metamagnetic Transition in Heavy Fermion Superconductor* UTe_2, J. Phys. Soc. Jpn. **88**, 063706 (2019).
[47] S. Imajo, Y. Kohama, A. Miyake, C. Dong, M. Tokunaga, J. Flouquet, K. Kindo, and D. Aoki, *Thermodynamic Investigation of Metamagnetism in Pulsed High Magnetic Fields on Heavy Fermion Superconductor* UTe_2, J. Phys. Soc. Jpn. **88**, 083705 (2019).
[48] A. Miyake, Y. Shimizu, Y. J. Sato, D. Li, A. Nakamura, Y. Homma, F. Honda, J. Flouquet, M. Tokunaga, and D. Aoki, *Enhancement and Discontinuity of Effective Mass through the First-Order Metamagnetic Transition in* UTe_2, J. Phys. Soc. Jpn. **90**, 103702 (2021).
[49] S. K. Yip, T. Li, and P. Kumar, *Thermodynamic Considerations and the Phase Diagram of Superconducting* UPt_3, Phys. Rev. B **43**, 2742 (1991).
[50] A. Miyake, M. Gen, A. Ikeda, K. Miyake, Y. Shimizu, Y. J. Sato, D. Li, A. Nakamura, Y. Homma, F. Honda, J. Flouquet, M. Tokunaga, and D. Aoki, *Magnetovolume Effect on the First-Order Metamagnetic Transition in* UTe_2, J. Phys. Soc. Jpn. **91**, 063703 (2022).
[51] D. Li, A. Nakamura, F. Honda, Y. J. Sato, Y. Homma, Y. Shimizu, J. Ishizuka, Y. Yanase, G. Knebel, J. Flouquet, and D. Aoki, *Magnetic Properties under Pressure in Novel Spin-Triplet Superconductor* UTe_2, J. Phys. Soc. Jpn. **90**, 073703 (2021).
[52] C. P. Bean, *Magnetization of High-Field Superconductors*, Rev. Mod. Phys. **36**, 31 (1964).
[53] V. V. Eremenko, V. A. Sirenko, H. Szymczak, and A. Nabialek, *Magnetostriction of Superconductors (A Review)*, Low Temp. Phys. **25**, 225 (1999).
[54] C. Paulsen, G. Knebel, G. Lapertot, D. Braithwaite, A. Pourret, D. Aoki, F. Hardy, J. Flouquet, and J.-P. Brison, *Anomalous Anisotropy of the Lower Critical Field and Meissner Effect in* UTe_2, Phys. Rev. B **103**, L180501 (2021).
[55] S. Kittaka, Y. Shimizu, T. Sakakibara, A. Nakamura, D. Li, Y. Homma, F. Honda, D. Aoki, and K. Machida, *Orientation of Point Nodes and Nonunitary Triplet Pairing Tuned by the Easy-Axis Magnetization in* UTe_2, Phys. Rev. Res. **2**, 032014(R) (2020).
[56] Generally speaking, in electrical transport measurements, filamentary superconductivity easily leads to slightly higher T_c values. However this filamentary superconductivity is fragile under small fields; hence, it is usual to observe a small positive curvature of H_{c2} determined by resistivity. In UTe_2, it may mask the negative curvature of H_{c2} clearly visible in Fig. 8 close to T_c.
[57] V. Mineev, *Upper Critical Field in Ferromagnetic Metals with Triplet Pairing*, Ann. Phys. (Amsterdam) **417**, 168139 (2020).
[58] K. Willa, F. Hardy, D. Aoki, D. Li, P. Wiecki, G. Lapertot, and C. Meingast, *Thermodynamic Signatures of Short-Range Magnetic Correlations in* UTe_2, Phys. Rev. B **104**, 205107 (2021).
[59] Q. Niu, G. Knebel, D. Braithwaite, D. Aoki, G. Lapertot, M. Vališka, G. Seyfarth, W. Knafo, T. Helm, J.-P. Brison, J. Flouquet, and A. Pourret, *Evidence of Fermi Surface Reconstruction at the Metamagnetic Transition of the Strongly Correlated Superconductor* UTe_2, Phys. Rev. Res. **2**, 033179 (2020).
[60] N. R. Werthamer, E. Helfand, and P. C. Hohenberg, *Temperature and Purity Dependence of the Superconducting CriticalFfield,* H_{c2}. *III. Electron Spin and Spin-Orbit Effects*, Phys. Rev. **147**, 295 (1966).
[61] K. Hasselbach, L. Taillefer, and J. Flouquet, *Critical Point in the Superconducting Phase Diagram of* UPt_3, Phys. Rev. Lett. **63**, 93 (1989).
[62] S. Khim, J. F. Landaeta, J. Banda, N. Bannor, M. Brando, P. M. R. Brydon, D. Hafner, R. Küchler, R. Cardoso-Gil, U. Stockert, A. P. Mackenzie, D. F. Agterberg, C. Geibel, and E. Hassinger, *Field-Induced Transition within the Superconducting State of* $CeRh_2As_2$, Science **373**, 1012 (2021).
[63] J. F. Landaeta, P. Khanenko, D. C. Cavanagh, C. Geibel, S. Khim, S. Mishra, I. Sheikin, P. M. R. Brydon, D. F. Agterberg, M. Brando, and E. Hassinger, *Field-Angle Dependence Reveals Odd-Parity Superconductivity in* $CeRh_2As_2$, Phys. Rev. X **12**, 031001 (2022).
[64] G. Knebel, M. Kimata, M. Vališka, F. Honda, D. X. Li, D. Braithwaite, G. Lapertot, W. Knafo, A. Pourret, Y. J. Sato, Y. Shimizu, T. Kihara, J. P. Brison, J. Flouquet, and D. Aoki, *Anisotropy of the Upper Critical Field in the Heavy-Fermion Superconductor* UTe_2 *under Pressure*, J. Phys. Soc. Jpn. **89**, 053707 (2020).
[65] S. Ran, H. Kim, I.-Lin Liu, S. R. Saha, I. Hayes, T. Metz, Y. S. Eo, J. Paglione, and N. P. Butch, *Enhancement and Reentrance of Spin Triplet Superconductivity in* UTe_2 *under Pressure*, Phys. Rev. B **101**, 140503(R) (2020).
[66] K. Kinjo, H. Fujibayashi, S. Kitagawa, K. Ishida, Y. Tokunaga, H. Sakai, S. Kambe, A. Nakamura, Y. Shimizu, Y. Homma, D. X. Li, F. Honda, D. Aoki, K. Hiraki, M. Kimata, and T. Sasaki, *Magnetic Field-Induced Transition with Spin Rotation in the Superconducting Phase of* UTe_2, arXiv:2206.02444.
[67] H. Sakai, Y. Tokiwa, P. Opletal, M. Kimata, S. Awaji, T. Sasaki, D. Aoki, S. Kambe, Y. Tokunaga, and Y. Haga, *Field Induced Multiple Superconducting Phases in* UTe_2 *along Hard Magnetic Axis*, arXiv:2210.05909.
[68] Y. Yu and S. Raghu, *Quenched Randomness, Thermal Fluctuations, and Reentrant Superconductivity: Application to* UTe_2, Phys. Rev. B **105**, 174506 (2022).
[69] B. Wu, D. Aoki, and J.-P. Brison, *Vortex Liquid Phase in the p-Wave Ferromagnetic Superconductor UCoGe*, Phys. Rev. B **98**, 024517 (2018).
[70] F. Guillou, A. K. Pathak, D. Paudyal, Y. Mudryk, F. Wilhelm, A. Rogalev, and V. K. Pecharsky, *Non-Hysteretic First-Order Phase Transition with Large Latent Heat and Giant Low-Field Magnetocaloric Effect*, Nat. Commun. **9**, 2925 (2018).
[71] Y. Yanase (private communication).

[72] A. B. Shick and W. E. Pickett, *Spin-Orbit Coupling Induced Degeneracy in the Anisotropic Unconventional Superconductor* UTe_2, Phys. Rev. B **100**, 134502 (2019).

[73] D. Aoki, T. Combier, V. Taufour, T. D. Matsuda, G. Knebel, H. Kotegawa, and J. Flouquet, *Ferromagnetic Quantum Critical Endpoint in UCoAl*, J. Phys. Soc. Jpn. **80**, 094711 (2011).

[74] D. Aoki, W. Knafo, and I. Sheikin, *Heavy Fermions in a High Magnetic Field*, C. R. Phys. **14**, 53 (2013).

[75] U. Rauchschwalbe, U. Ahlheim, F. Steglich, D. Rainer, and J. J. M. Franse, *Upper Critical Magnetic Fields of the Heavy Fermion Superconductors* $CeCu_2Si_2$, UPt_3, *and* UBe_{13}*: Comparison between Experiment and Theory*, Z. Phys. B **60**, 379 (1985).

[76] Y. Shimizu, D. Braithwaite, D. Aoki, B. Salce, and J.-P. Brison, *Spin-Triplet p-Wave Superconductivity Revealed under High Pressure in* UBe_{13}, Phys. Rev. Lett. **122**, 067001 (2019).

[77] F. Hardy and A. D. Huxley, *p-Wave Superconductivity in the Ferromagnetic Superconductor URhGe*, Phys. Rev. Lett. **94**, 247006 (2005).

[78] S. Belin, T. Shibauchi, K. Behnia, and T. Tamegai, *Probing the Upper Critical Field of* κ-$(BEDT\text{-}TTF)_2Cu(NCS)_2$, J. Supercond. **12**, 497 (1999).

[79] G. Grissonnanche, O. Cyr-Choinière, F. Laliberté, S. Renéde Cotret, A. Juneau-Fecteau, S. Dufour-Beauséjour, M. È. Delage, D. LeBoeuf, J. Chang, B. J. Ramshaw *et al.*, *Direct Measurement of the Upper Critical Field in Cuprate Superconductors*, Nat. Commun. **5**, 3280 (2014).

[80] A. E. Koshelev, K. Willa, R. Willa, M. P. Smylie, J.-K. Bao, D. Y. Chung, M. G. Kanatzidis, W.-K. Kwok, and U. Welp, *Melting of Vortex Lattice in the Magnetic Superconductor* $RbEuFe_4As_4$, Phys. Rev. B **100**, 094518 (2019).

[81] F. Thomas, B. Wand, T. Lühmann, P. Gegenwart, G. R. Stewart, F. Steglich, J. P. Brison, A. Buzdin, L. Glémot, and J. Flouquet, *Strong Coupling Effects on the Upper Critical Field of the Heavy-Fermion Superconductor* UBe_{13}, J. Low Temp. Phys. **102**, 117 (1996).

[82] L. N. Bulaevskii, O. V. Dolgov, and M. O. Ptitsyn, *Properties of Strong-Coupled Superconductors*, Phys. Rev. B **38**, 11290 (1988).

[83] Y. S. Eo, S. Liu, S. R. Saha, H. Kim, S. Ran, J. A. Horn, H. Hodovanets, J. Collini, T. Metz, W. T. Fuhrman, A. H. Nevidomskyy, J. D. Denlinger, N. P. Butch, M. S. Fuhrer, L. A. Wray, and J. Paglione, *c-Axis Transport in* UTe_2*: Evidence of Three-Dimensional Conductivity Component*, Phys. Rev. B **106**, L060505 (2022).

[84] G. J. McMullan, P. M. C. Rourke, M. R. Norman, A. D. Huxley, N. Doiron-Leyraud, J. Flouquet, G. G. Lonzarich, A. McCollam, and S. R. Julian, *The Fermi Surface and* f*-Valence Electron Count of* UPt_3, New J. Phys. **10**, 053029 (2008).

[85] G. Bastien, D. Aoki, G. Lapertot, J.-P. Brison, J. Flouquet, and G. Knebel, *Fermi-Surface Selective Determination of the g-Factor Anisotropy in* URu_2Si_2, Phys. Rev. B **99**, 165138 (2019).